AEDC-TR-90-26

C.3

Nonintrusive Nitric Oxide Density Measurements in the NASA Langley Arc-Heated Scramjet Engine Test Facility

R. P. Howard, K. L. Dietz, W. K. McGregor,
and
C. C. Limbaugh
Sverdrup Technology, Inc.

January 1991

Final Report for Period April 1, 1988 through June 1, 1990

ARNOLD ENGINEERING DEVELOPMENT CENTER
ARNOLD AIR FORCE BASE, TENNESSEE
AIR FORCE SYSTEMS COMMAND
UNITED STATES AIR FORCE

NOTICES

When U. S. Government drawings, specifications, or other data are used for any purpose other than a definitely related Government procurement operation, the Government thereby incurs no responsibility nor any obligation whatsoever, and the fact that the Government may have formulated, furnished, or in any way supplied the said drawings, specifications, or other data, is not to be regarded by implication or otherwise, or in any manner licensing the holder or any other person or corporation, or conveying any rights or permission to manufacture, use, or sell any patented invention that may in any way be related thereto.

Qualified users may obtain copies of this report from the Defense Technical Information Center.

References to named commercial products in this report are not to be considered in any sense as an endorsement of the product by the United States Air Force or the Government.

This report has been reviewed by the Office of Public Affairs (PA) and is releasable to the National Technical Information Service (NTIS). At NTIS, it will be available to the general public, including foreign nations.

APPROVAL STATEMENT

This report has been reviewed and approved.

CARLOS TIRRES
Propulsion Division
Directorate of Technology
Deputy for Operations

Approved for publication:

FOR THE COMMANDER

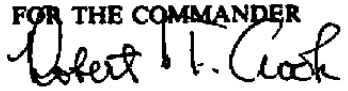

ROBERT T. CROOK
Acting Director of Technology
Deputy for Operations

REPORT DOCUMENTATION PAGE

Form Approved
OMB No. 0704-0188

1 AGENCY USE ONLY (Leave blank)	2 REPORT DATE	3 REPORT TYPE AND DATES COVERED
	January 1991	Final, April 1, 1988 -- June 1, 1990

4 TITLE AND SUBTITLE

Nonintrusive Nitric Oxide Density Measurements in the NASA Langley Arc-Heated Scramjet Engine Test Facility

5 FUNDING NUMBERS

PE-65807F

C-F40600-85-C-0026

6 AUTHOR(S)

Howard, R. P., Dietz, K. L., McGregor, W. K., and Limbaugh,C. C., Sverdrup Technology, Inc., AEDC Group

7 PERFORMING ORGANIZATION NAME(S) AND ADDRESS(ES)

Arnold Engineering Development Center/DOT
Air Force Systems Command
Arnold AFB, TN 37389-5000

8 PERFORMING ORGANIZATION REPORT NUMBER

AEDC-TR-90-26

9 SPONSORING/MONITORING AGENCY NAMES(S) AND ADDRESS(ES)

Arnold Engineering Development Center/DO
Air Force Systems Command
Arnold AFB, TN 37389-5000

10 SPONSORING/MONITORING AGENCY REPORT NUMBER

11 SUPPLEMENTARY NOTES

Available in Defense Technical Information Center (DTIC).

12a DISTRIBUTION/AVAILABILITY STATEMENT

Approved for public release; distribution is unlimited.

12b. DISTRIBUTION CODE

13. ABSTRACT (Maximum 200 words)

A nitric oxide (NO) resonance absorption technique was used to determine average path integrated NO number densities through the expanded flow of the NASA Langley Arc-Heated Scramjet Test Facility. The mole fraction ranged from 0.016 to 0.019 (with a 20-percent uncertainty) for static temperatures from 186 to 320 K. Absorption was observed in the NO gamma (0,1) band that could not be accounted for at the static flow conditions if the NO were at vibrational equilibrium. Using the (0,1) transmittance measurement and the number density calculated from the (0,0) transmittance measurement, vibrational temperatures ranging from 534 to 919 K were calculated with a minimum uncertainty from −15 to 21 percent. A nonequilibrium vibrational temperature, 1,100 K, was calculated from a one-dimensional kinetic (ODK) chemistry code compared to the 919 K determined from the measurement. Within the range of uncertainties of the (0,1) absorption measurements, the corresponding NO radiative transfer code calculations of vibrational temperature, and the range of uncertainties of the ODK code calculations, there is good agreement in the resulting vibrational temperatures.

14 SUBJECT TERMS		15. NUMBER OF PAGES
arc heater	**resonance absorption**	**69**
NO gamma bands	**vibrational nonequilibrium**	16 PRICE CODE
nitric oxide	**vibrational relaxation**	

17 SECURITY CLASSIFICATION OF REPORT	18 SECURITY CLASSIFICATION OF THIS PAGE	19 SECURITY CLASSIFICATION OF ABSTRACT	20 LIMITATION OF ABSTRACT
UNCLASSIFIED	**UNCLASSIFIED**	**UNCLASSIFIED**	**SAME AS REPORT**

PREFACE

The research reported herein was performed by the Arnold Engineering Development Center (AEDC), Air Force Systems Command (AFSC). Work and analysis for this research were done by personnel of Sverdrup Technology, Inc., AEDC Group, operating contractor for the AEDC propulsion test facilities, under Project Number DC80EW. The Sverdrup Project Manager was K. L. Dietz, and the Air Force Project Manager was C. Tirres. The data measurement and initial analysis was completed on May 1, 1989. Additional analysis was completed June 1, 1990. This report was submitted for publication on December 11, 1990.

The authors wish to express their appreciation for the contributions made by G. Burton Northam, Olin Jarrett, Jr., Scott R. Thomas, R. Wayne Guy, and Randall T. Voland of the NASA Langley Research Center.

CONTENTS

ILLUSTRATIONS

TABLES

APPENDIXES

1.0 INTRODUCTION

Nitric oxide, NO, is produced in arcs used for heating air to the high temperatures required for hypersonic aerodynamic and propulsion test facilities. Although there is NO in the flight environment, its concentration is far below that produced in the test facilities. It is known that the NO molecule plays a role in the heating of aerodynamic surfaces in hypersonic flow and an even greater role in the combustion kinetics of hypersonic air-breathing engines (ramjets and scramjets). Thus, it becomes vitally important to know the concentration of this species in the test facility flow so that flight performance may be adequately determined from the ground test results.

An ultraviolet (UV) resonance absorption method developed for measurements of NO concentration in turbine engine exhausts (Refs. 1 and 2) has been adapted for arc-heated flows. The concentration in arc-heated flows is on the order of a few percent, whereas the NO concentration in turbine engine exhausts is generally much lower and on the order of a few hundred parts per million. At the higher NO densities of the arc-heated flows, the NO gamma (0,0) band absorption may become saturated, and the NO gamma (0,1) band can be used. The radiative transfer model, used to determine NO number densities from transmittance measurements, was extended to include the absorption in this band. Instrument improvements included using a linear array detector, or optical multichannel analyzer (OMA), for the spectral dispersing instrument rather than scanning a grating as used in the earlier work. The instrument response function is an integral part of the radiative transfer model. The model was extended to include the OMA response function.

Application of the modified instrumentation and data reduction procedures was made in the NASA Langley Arc-Heated Scramjet Test Facility (Refs. 3 and 4), and path-integrated NO densities were determined for a number of test conditions. This report describes the instrument and model extensions and the results of the experimental determinations. Additionally, comparisons are made to the vibrational distribution predictions of a one-dimensional relaxation code.

2.0 APPARATUS

The measurements reported herein were accomplished in the NASA Langley Arc-Heated Scramjet Test Facility with the Mach 6 nozzle. The facility is described in detail in Refs. 3, 4, and 5. A schematic of the arc heater, plenum chamber, and Mach 6 nozzle from these references is given in Fig. 1. Briefly, approximately 4,700 K total temperature arc-heated air is mixed in the plenum chamber with a stream of unheated bypass air and expanded through the contoured square-cross-section Mach 6 nozzle into the test section of the facility. The throat area is about 8.44 cm^2, and the nozzle expands to an area of about 765 cm^2 in an

axial length of 157 cm. A diffuser downstream of the test section reduces the gas velocity to subsonic velocity. The gas is cooled and exhausted into a vacuum sphere. The airflow is established seconds before the arc heater is powered on. The facility is operated nominally 45 sec/test.

The facility operating conditions for the tests conducted for the present work are given in Table 1. The tests are labeled using a Run (R) and Batch (B) notation used at the NASA facility. The "R" denotes a particular facility test period in which the equipment was in readiness for testing, typically a single day. The "B" denotes an actual set of conditions at which the facility was operated, and data were collected and numbered sequentially within the "R" period. Thus, R2B2 data were acquired after R2B1 data but in the same test period, and R3B1 data were acquired on a later day. The "main air" is air introduced into the heater. "Bypass air" is ambient-temperature air used to dilute the arc-heated air in the plenum chamber. H_t, T_t, and P_t are the facility bulk enthalpy, total temperature, and total pressure, respectively, in the plenum chamber. T_s and P_s are the test flow free-stream static temperature and pressure, respectively, at the exit of the nozzle. T_s and P_s of Table 1 are approximations of the static temperature and pressure at the position of the resonance absorption measurements through the nozzle.

3.0 NO RESONANCE ABSORPTION SYSTEM

The NO resonance absorption system consists of the instrumentation to perform transmittance measurements and a theoretical radiative transfer modeling code to interpret NO concentrations from the measurement.

3.1 INSTRUMENTATION

The NO measurement system consists of an NO resonance lamp emission source, fiber optics and lenses to direct the lamp emissions, and a spectrometer/OMA detector system. The major components of the NO resonance absorption system instrumentation and its relation to the facility nozzle are illustrated in Fig. 2. The NO radiation source lamp is a DC- excited, water-cooled, capillary discharge tube. A 12:3:1 gas mixture (by volume) of argon, nitrogen, and oxygen, respectively, flows through the tube at a static pressure of 10 torr. The lamp discharge is sustained by a current-regulated power supply operating at 11-ma current and 5,000 V with a 207-kΩ ballast resistance.

A UV-grade optical fiber (600-μm core) is used to direct the source radiation to the test airflow. UV-grade fused silica windows provide optical access to the nozzle through two, 2.54-cm-diam ports on the nozzle wall located 5.7 cm below centerline and 43.2 cm from the nozzle exit as shown in Fig. 1. The source radiation is collimated to a 1.9-cm-diam beam

by a lens exterior to the nozzle, passes through the optical ports of the nozzle, and is transmitted through an identical focusing lens and optical fiber arrangement to the spectrometer receiving optics. The beam from the fiber is focused onto the spectrometer entrance slit as it is reflected from an optical bandpass reflection filter. The reflection filter is used to isolate the NO radiation and reduce the stray light. The peak reflection efficiency of the filter was 91 percent at 240 nm with a 30-nm full-width-half-maximum (FWHM) bandpass.

The receiver was a 0.32-m Czerny-Turner configuration spectrometer with a 25-μm entrance slit. The diffracting element was a ruled 1,800 groove/mm plane grating used in first order, giving a spatial dispersion of 1.52 nm/mm in the exit plane of the spectrometer. The detector was an EG&G PAR[e] Model 1421-B, UV-enhanced, intensified silicon photodiode array (See Appendix A). The detector array had 1,024 pixels (detector elements), each 2.5 mm tall by 25 μm wide on 25-μm centers. With the detector installed, the FWHM spectral resolution was 0.19 nm. The spectral range covered by the detector was slightly less than the reflection filter bandpass and ranged from 223 to 260 nm, which included the NO gamma (0,0), (0,1), (0,2), and (0,3) vibrational bands.

3.2 INSTRUMENT AND LAMP CHARACTERISTICS

Proper use of the resonance absorption system requires laboratory characterization of the source and detector. The lamp radiation is the result of a high-voltage discharge. As described in Ref. 2, it is unreasonable to expect the emitted spectral line intensities to follow thermal equilibrium considerations. Rather, the lines must be individually characterized at the lamp operating conditions. For this calibration, high-resolution spectra of both the (0,0) and (0,1) bands were measured in the laboratory using a 1-m grating spectrometer with a spectral resolution of 0.0045 nm. A characterization curve as described in Ref. 2 was generated for each band from the resolved lines. Each curve is a plot of the radiation intensity ($I_{J'J''}$) divided by the relative line strength ($\delta_{J'J''}$) versus the upper-state energy ($F_{J'}$), where J′ and J′′ are the rotational quantum numbers of the upper and lower energy states for a transition, respectively. Intensities for transitions not resolvable within a band are interpolated from this curve according to the upper-state energy of the rotational transition. These lamp characterization curves were used in modeling the resource radiation during data analysis. Also the presence of the argon in the source working gas provides a low level of continuum in the emitted radiation from the lamp. Consequently, as described in the following, this continuum was included in the model.

An important instrument characterization necessary to model the absorption measurement is the instrument response function for each detector element used in the determination of number density. The normalized response for each element was determined by recording the signal level of the detector element since a singlet-transition mercury (Hg) line was scanned

across the detector array in the exit plane of the spectrometer. For example, Fig. 3 shows the relative response for Detector Element 39 (which is located spectrally at the second bandhead of the (0,0) band). As the Hg line was scanned away from this detector, the response reduced by one order of magnitude within 2 adjacent detector elements (0.076 nm) and gradually decreased beyond 4 detector elements. The intensifier component of the detector is believed to be the cause of a measurable response beyond a few adjacent detector elements. In the present work, the instrument response for a detector was determined insignificant beyond 20 detector elements. It should be noted parenthetically that the response shown in Fig. 3 for Detector Element 39 is asymmetrical because the element is near the edge of the detector array. Instrument response functions for detector elements away from the edge were symmetrical about the center detector element.

3.3 THEORETICAL MODELING CODE

A computer model based on the theoretical line-by-line radiative transfer model for the NO gamma (0,0) and (0,1) electronic-vibrational bands of the NO molecule was used to analyze the transmittance measurements through the test media. Generally, for a given total static pressure, static temperature, and path length, data are reduced by varying the NO concentration until the calculated and measured transmittances agree. Although the code can be used for inversion for profiles of plume properties when appropriate data are taken, the present measurements were for a single line-of-sight. Consequently, the data are reduced as if from a homogeneous medium with a uniform temperature and pressure. The resulting NO concentration is interpreted as a single, average concentration over the line-of-sight measurement volume.

A detailed discussion of the theory and computer code can be found in Refs. 1 and 2. Theoretical parameters necessary in extending the modeling code to calculate absorption in the (0,1) band were taken from the literature. The band center wavenumber, 42191.0 cm^{-1}, was used in calculating the line center absorption coefficient. The rotational constant, 1.6783 cm^{-1} (Ref. 6), is vibrationally dependent. The most recent value, 5.84×10^{-4}, calculated from Eq. (5) of Ref. 7 was used for the band oscillator strength. The spectral line positions published by Deezsi (Ref. 8) were used for both the (0,0) and (0,1) bands. The lamp characteristics for each line as described previously were incorporated into the code to model the relative intensities of the source rotational transitions.

The modification for the argon continuum required that the spectral region of the bands be modeled at increments small enough to include spectral features of both the source and absorption media rotational transitions. The source and absorption transitions were modeled by Doppler and Voigt profiles, respectively. The intensity of the argon continuum varies spectrally, but is approximately constant over the spectral region of the instrument response

at the second bandhead of an NO gamma band. Thus, the argon continuum is modeled by different values of its intensity, I_c, for the (0,0) and (0,1) bands, respectively. The code parameter I_c also compensates for possible scattered radiation within the spectrometer.

The NO broadening parameter (Ref. 2) is given by

$$a' = C(P_s/T_s^n)$$

where P_s and T_s are static pressure and temperature, respectively, n is a temperature exponent that gives the best curve fit to experimental data, and C is the broadening constant. Both a' and I_c were used as code calibration parameters to assure that the code calculations and laboratory transmittance measurements agreed.

The code parameter value of I_c depends upon stray light within the spectrometer. If the lamp signal is much greater than the test media emission, a necessary condition for reliability in applications as described with the present instrumentation, the primary source of potential stray light is the source lamp. Thus, it is important that the instrument configuration during calibration be maintained during test measurements, especially the use of filters.

The code calibration parameters for the (0,0) band were determined from transmittance measurements made through a 7.37-cm quartz absorption cell at static temperatures from 300 to 500 K, total static pressures from 0.0132 to 0.132 atm, and NO gas mixtures of 0.14, 0.8, and 1.98 percent by volume (N_2 as the diluent gas). Because of the low absorption at low temperatures, code calibration parameters for the (0,1) band were obtained for cell static temperatures from 600 to 950 K and static pressures from 0.066 to 0.25 atm using these gas mixtures. Laboratory measurements were repeatable within a transmittance of 0.008. The NO number densities are deduced from the transmittance measured at the detector element for which the pretest lamp reference intensity, at the respective (0,0) or (0,1) second bandhead, is a maximum. For the present work, good agreement was achieved between measured and code-calculated transmittances by using the value of C = 38,100 and n = 1.5 (See Ref. 2) for both the (0,0) and (0,1) bands to determine a', and varying I_c independently for each band until a best overall match of calculated-to-measured transmittances was found. The values of I_c equal to 25 and 4 were ultimately determined for the (0,0) and (0,1) bands, respectively. Using these values, the code accurately predicted the NO number density to within 25 percent over the range of conditions described previously.

It is not surprising that the previously published values of a' work well because of the similarity in lamp design and lamp operating conditions from the previous work. The characterization of the present lamp was accomplished independently of Ref. 2 for both the (0,0) and (0,1) bands. The characterization of the (0,0) band agrees well with the results in Ref. 2.

It should be emphasized that a′ and I_c are instrument-dependent code calibration parameters and should not be interpreted otherwise. Also, number densities calculated for conditions far outside the range of calibration conditions described herein have unknown uncertainties.

To confirm the code calibrations for the (0,0) band at a longer pathlength, transmission measurements were made in the laboratory through a 33-cm stainless steel absorption cell with sapphire windows. The temperature was maintained at 298 K. The code accurately predicted the NO number density to within 20 percent for a 1.98-percent NO mixture (diluted with nitrogen) at 0.0132, 0.264, 0.66, and 1.32 atm.

4.0 VIBRATION RELAXATION CODE

The vibrational relaxational calculations are accomplished using a one-dimensional kinetic (ODK) chemistry code modified for vibrational relaxation calculations as described previously (Ref. 9). To summarize, the ODK code calculates the inviscid, chemically reacting nozzle expansions of gaseous exhaust mixtures. The results of a chemical equilibrium code for the plenum chamber are used as initial values. In principle, there is no requirement that the species be distinct chemical species. Treating each excited vibrational state as a separate species allows one to calculate the development of the state densities in an expanding flow. Including the appropriate rate coefficients in a finite-rate chemistry gas-dynamic code allows examination of the internal distribution of states as the gas flow develops along the nozzle. In this manner, a non-Boltzmann vibrational distribution will manifest itself as a natural result when the collision frequency becomes too low to maintain a particular state in collisional equilibrium with the rest of the ensemble. The specific version of the code allowed up to 150 chemical reactions and 48 species or vibrational states.

Proper utilization of a finite-rate chemistry code for vibrational relaxation calculations requires that distinct vibrational states for the constituent molecules be maintained as separate and distinct species. For air species in the flows considered here, the important species for relaxation are the diatomic molecules N_2, O_2, and NO. Since there is a practical limit to the number of vibrational states that can be used to describe a molecule in the computations, only those states through vibrational quantum Level 3 were kept separate and distinct. The additional upper-state densities were included in an upper level (designated "U") at an energy of vibrational Level 4 to provide a reservoir for filling the upper distinct state. The energy levels for the diatomic molecules were calculated using molecular parameters from Huber and Herzberg (Ref. 10). The upper lying vibrational states, U, are assumed to be in thermal equilibrium with the rest of the gas. Since collisional numbers for rotational equilibration are generally near the same as for translational equilibration, the rotational levels were assumed to be in a Boltzmann distribution at the gas temperature.

Ionic reactions were not included here since the principal concern is for relaxation for the major species. The NO^+ recombination reaction results in the formation of the N and O atoms, which will subsequently chemically react to form NO, N_2, or O_2. Further, the initial conditions in the plenum chamber for this work are considered to be thermal equilibrium, and the mole fractions of the ionic species at the conditions studied here were small. Consequently, although it is ultimately important for a complete chemistry description of the arc-heated airflow, at this initial stage the effects of exclusion of the ionic reactions will have little effect on the results of the study. Higher plenum chamber temperatures or the utilization of nonequilibrium distributions for initial conditions would require their consideration.

Rate coefficients for vibration-translation (V-T) and vibration-vibration (V-V) for the N_2 and O_2 reactions were taken from a review by Blauer and Nickerson (Ref. 11) and for the NO reactions from a review by Lewis and Trainor (Ref. 12). The two reviews complement each other. The rate coefficients available are generally for lower state reactions only. Higher-state transitions were approximated for the present work using the simple harmonic oscillator potential.

Radiative transitions are not included in the present relaxation calculations. Chemical transformation reactions (e.g., $N + N = N_2$) are assumed to form the product molecules in the U state. V-T reactions between a species in the U state and the next higher vibrational state are assumed to proceed at collision speed; i.e., with a collision number of one. This assumption is conservative in that it assures that the two upper, excited states are maintained in a thermal distribution. For example, Ref. 13 shows the vibrational relaxation of N_2 can require collision numbers several orders of magnitude greater than one. Thus, the U states act as a reservoir for the relaxation, feeding into the lower state distribution through the State 3 as required to maintain a local-thermodynamic-equilibrium (LTE) value with the State 3. Consequently, the non-LTE (NLTE) distribution in the present study arises because of the low reaction rates involving the lower states. Inclusion of more states with correct rate coefficients would likely increase the effects of the relaxation.

5.0 TEST CONDITIONS AND DATA

Data were acquired on 12 tests at the facility operating conditions summarized in Table 1 (personal communication from Scott R. Thomas, NASA Langley Research Center, April 1989). The test conditions of Table 1 are listed in the order that the tests were performed, except for tests R2B3, R4B1, and R4B4. These are listed separately in the table because of an anomaly to be discussed later. The facility conditions for Test R3B3 were repeated in Tests R4B2 and R4B3. Also, facility conditions for test R2B3 were repeated in Tests R4B1 and R4B4. Data representative of the 12 tests are presented in the present discussion. Data typical of each test are given in Appendix B.

Figure 4 shows typical uncorrected lamp spectra before and during arc-heated flow. Figure 4a shows the entire spectral range covered by the detector array, and Fig. 4b shows the portion of the spectrum covering the (0,0) and (0,1) bands only. Absorption in the (0,0) and (0,1) bands by the arc-heated flow is obvious in Fig. 4b. At the anticipated densities of the flow, and assuming thermal equilibrium, absorption in the (0,1) band is not expected at the low static temperatures of the flow. Thus, one infers that the NO distribution had frozen at a higher vibrational temperature upstream of the measurement point.

Figure 5 shows a typical pretest background scan (Fig. 5a) and an emission scan plus background (Fig. 5b) during arc-heated flow. As is seen in Fig. 5b, there was no measurable emission from the airflow. The small amount of signal above background (hardly distinguishable on the scale of Fig. 5b) is attributable to a persistence of the detector signal, a normal condition in the intensifier of the detector called "phosphor lag." The error introduced by this small signal is much smaller than other normal measurement uncertainties.

Figure 6 illustrates a time history of significant events during data acquisition that is typical of the first 9 tests shown in Table 1. In this figure the intensities at the second bandhead of the (0,0) and first bandhead of the (0,3) bands are plotted as a function of time (scan number) for Test R2B1. As shown in Figs. 6a and b, the lamp was initially shuttered to obtain a pretest background signal level, then opened to measure a pretest lamp reference level I_0. As the facility airflow began, the signals were attenuated by condensation of the airflow constituents in the line-of-sight because of the rapid expansion of the cold airflow in the nozzle. When the arc was established, the (0,3) signal returned to the pretest level, indicating neither attenuation nor absorption, whereas the (0,0) signal decreased to an appropriate level because of NO absorption. During the arc-heated flow, the lamp was shuttered to measure emission levels from the flow. As the arc was extinguished, the (0,0) signal increased and the (0,3) signal decreased consistent with cold-air attenuation signal levels. When the flow was discontinued, the signal levels at the (0,0) and (0,3) bands returned to their respective pretest levels. Although a time history for the (0,1) band is not presented, the signal level of the (0,1) band exhibited the same characteristics as the (0,0) band during the test.

During the initial tests, R1B1, R2B1, R2B2, and R2B3, 0.5-sec detector integration times were used. The transmission of the lamp was observed to be constant within the noise level of the measurement over the duration of the test. Consequently, to reduce the amount of data to be acquired and stored, the integration time was set to 1 sec in subsequent tests.

Data such as is shown in Figs. 4 and 5 were reduced to transmittance, τ, as follows:

$$\tau = (I_T - I_B) / (I_0 - I_B)$$

where I_T is a lamp scan taken through the arc-heated flow, I_0 is a lamp reference scan, and I_B is the pretest background scan. A typical plot of transmittance, R4B3, is shown in Fig. 7. For each test, when possible, spectra were averaged (during steady-state conditions) to increase the signal-to-noise ratio. Lamp reference spectra were acquired both pretest (before airflow was begun) and posttest (after airflow was shut off). In all but the first test, R1B1, pretest and posttest lamp reference levels were the same. For Test R1B1, the resulting transmittance data were necessarily adjusted to give a transmittance value of 1.0 outside the spectral regions of the (0,0) and (0,1) bands. Although these adjustments were small for the other test spectra, the transmittances at the (0,0) and (0,1) bandheads were corrected for possible lamp-time variations in a similar way. The adjusted transmittance at the second bandhead for both the (0,0) and (0,1) bands, as well as other derived properties described in the following, are given in Table 2 for each of the 12 tests.

The last three tests of Table 1, all with similar facility operation conditions, showed a different transient characteristic and required special handling of the data. To illustrate the reason for the special considerations, example time-dependent data from Test R4B4, representative of the last 3 tests described in Table 1, are given in Fig. 8. As in Fig. 6, the signal levels of the (0,0) and (0,3) bands were attenuated during the unheated airflow. However, the (0,3) band signal level did not return to the pretest level after the arc was established, indicating attenuation of the beam atypical of the other tests. A typical transmittance spectrum from these tests is shown in Fig. 9, measured during the arc-heated airflow of Test R4B1. The entire spectrum was attenuated. The total enthalpy for these tests was very low, resulting in nozzle exit static temperatures of less than 90 K, even with the arc operating. At these low static temperatures, condensation of residual H_2O, ambient CO_2, and/or O_2 in the airflow is possible, with consequent extinction of the beam. At these low enthalpies, there was no measurable NO absorption in the (0,1) band.

Since there were no spectral features on the transmittance curves to indicate NO absorption, except in the (0,0) band, the attenuation level outside the (0,0) spectral region was referenced as a transmittance of 1.0 with respect to NO absorption. This 100-percent reference for Test R4B1 is shown as a dashed line in Fig. 9. The resulting transmittance values for the (0,0) and (0,1) second bandheads are listed in Table 2 for the last 3 tests described in Table 1.

6.0 RESULTS

The transmittances derived from the measured data, the derived NO number densities, mole fractions, and vibrational temperatures are given in Table 2. The absorption path length through the nozzle used for these determinations was 27.66 cm. The radiative transfer model was used to determine the NO number density for each test condition of Table 1. The mole fractions of NO are calculated from the static temperatures and pressures from Table 1 using

the ideal-gas law. Mole fractions of NO ranged from 0.013 to 0.019 for the first nine tests and from 0.0017 to 0.0026 for the last three tests described in Table 1. Uncertainties of the derived densities are 20 percent for the first nine tests. Number densities determined for the last three tests of Table 1 have unknown uncertainties. Not only were unusual measures necessary to determine transmittances for these three tests, but the NO radiative transfer code has not been confirmed for such low static temperatures. Also, it should be noted that although the facility operating conditions for the last three tests were similar, the measured transmittance for R2B3 differs appreciably from the transmittances of R4B1 and R4B4.

As described previously, absorption of the (0,1) vibrational band at the static temperatures of the flow indicates that the NO has not achieved vibrational equilibrium at the region of the transmittance measurements. A vibrational temperature was determined based on the relative populations of the zero and first vibrational states of the ground electronic state of the NO molecule in the following manner. The NO radiative transfer model was used to determine the population (N_1) of the first vibrational state necessary to account for the (0,1) band absorption. To perform these calculations, a Boltzmann distribution characteristic of the flow static temperature was assumed for the rotational states. A vibrational temperature T_v was then determined from the Boltzmann distribution.

$$N_1/N_0 = \exp\left((E_1 - E_0) / kT_v\right)$$

where E_0 and E_1 are the vibrational energies of the zero and first vibrational states, respectively, and k is Boltzmann's constant. The results of these calculations are included in Table 2 for the first nine tests described in Table 1. The uncertainties in the calculated values of T_v, based upon the experimental transmittance uncertainties, were +21 and −15 percent.

As stated before, no measurable absorption was observed in the (0,1) band during the last three tests described in Table 1. Hence, vibrational temperatures could not be determined for these three cases.

A comparison of the vibrational relaxation calculations to the results of the density determinations for Test R3B4 is shown in Fig. 10. This case was chosen because it had the highest enthalpy and stagnation temperature. The results are presented as a Boltzmann plot in which the ordinate is the Log_{10} of the ratio of the upper-state density to the ground-state density. On a Boltzmann plot, those states that are in thermal equilibrium will fall on the same straight line. The lower line on the plot represents the slope of the line if the vibrational densities were in thermal equilibrium at the calculated static temperature of the gas. The line through the N_1 calculated point is at a vibrational temperature of 1,100 K. The experiment and calculation are in good agreement.

It is clear that both the calculated and experimentally derived densities deviate strongly from the LTE condition. Although not shown on Fig. 10, the vibrational distribution of N_2 and O_2 were also calculated and show even stronger deviations from thermal equilibrium. This is consistent with the observation (Ref. 13) that the V-V transitions of NO are much more efficient than for N_2 and O_2. The vertical bars on Fig. 10 with the calculation indicate the variation in the resultant calculated densities if the V-V and V-T rates are increased and decreased by a factor of two, respectively. The vertical bar with the data indicates the estimated uncertainty in the resultant experimentally determined density because of the experimental measurement uncertainty. Clearly, the calculations and data agree within the uncertainties.

It should be noted that the experimental NO number densities and the non-Boltzmann experimental vibrational temperatures are calculated from single, line-of-sight transmittance measurements. The results are average values over the measurement volume and do not take into account boundary-layer effects or flow anomalies that might be present. Although the magnitude for such effects cannot be quantified in the present study, qualitative effects may be inferred. Data acquired from a path that includes a hot, high-pressure narrow boundary layer interpreted as a long path average value would result in lower (0,1) densities than was actually the case. The (0,0) densities would not be affected to a large degree. Consequently, vibrational temperatures inferred from the vibrational temperatures reported in Table 2 should be viewed as a lower bound.

7.0 SUMMARY AND CONCLUSIONS

Transmittance measurements using an NO resonance source were reported for an expanded arc-heated flow. These data were used to deduce NO concentrations, which ranged from 0.17 to 1.9 percent by volume for facility operating conditions with nozzle exit static temperatures from 87 to 320 K and static pressures from 3.67×10^{-3} to 15.65×10^{-3} atm.

Absorption measurements in the (0,1) band, not attributable to a flow at thermal equilibrium, were used to calculate nonequilibrium vibrational temperatures that ranged from 533 to 919 K. These data were compared to vibrational distribution predictions of a one-dimensional relaxation code, which, within the uncertainties of calculations and measured transmittances, were in good agreement.

REFERENCES

1. Few, J. D., McGregor, W. K., and Glassman, H. N. "Resonance Absorption Measurements of NO Concentration in Combustor Exhausts." *AIAA Progress in Astronautics and Aeronautics—Experimental Diagnostics in Gas Phase Combustion Systems*. B.T. Zinn, Editor, AIAA Press, Princeton, New Jersey, 1977.

2. Davis, M. G., McGregor, W. K., and Few, J. D. "Utilizing the Resonance Line Absorption Technique to Determine the Collisional Broadening Parameters of a Diatomic Molecule: NO γ-Bands as an Example." *Journal of Quantitative Spectroscopy and Radiative Transfer*, Vol. 16, No. 12, December 1976, pp. 1109-1118.

3. Ostrander, M. J. et al. "CFD Simulation of Square Cross-Section, Contoured Nozzle Flows: Comparison with Data." AIAA Paper No. 89-0045, AIAA 27th Aerospace Sciences Meeting, January 9-12, 1989.

4. Thomas, Scott R., Voland, Randall, and Guy, Robert W. "Test Flow Calibration Study of the Langley Arc-Heated Scramjet Test Facility." AIAA Paper No. 87-2165, AIAA/SAE/ASME/ASEE 23rd Joint Propulsion Conference, June 29-July 2, 1987.

5. Thomas, Scott R. and Guy, Robert W. "Expanded Operational Capabilities of the Langley Mach 7 Scramjet Test Facility." NASA TP-2186, 1983.

6. Engleman, R., Jr. et al. "Beta and Gamma Systems for Nitric Oxide." Los Alamos Report LA-4364, July 1970.

7. Piper, L. G. and Cowles, L. M. "Einstein Coefficients and Transition Moment Variation for the NO($A^2\Sigma^+ - X^2\Pi$) Transition." *Journal of Chemical Physics*, Vol. 85, No. 5, September 1986, p. 2419.

8. Deezsi, I. "A Recent Rotational Analysis of the γ - Bands of the NO Molecule." *Acta Physica*, Vol. 9, 1957, p. 125.

9. Limbaugh, C. C. "Gas Diagnostics for High-Area-Ratio Rockets." AIAA Paper No. 85-1082, AIAA 20th Thermophysics Conference, Williamsburg, Virginia, June 19-21,1985.

10. Herzberg, G. and Huber, K. P. *Molecular Spectra and Molecular Structure: Volume IV. Constants of Diatomic Molecules.* van Nostrand Reinhold, New York, 1979.

11. Blauer, J. A. and Nickerson, G. R. "A Survey of Vibrational Relaxation Rate Data for Processes Important to CO_2 - N_2 - H_2O Infrared Plume Radiation." AIAA Paper No. 74-536, AIAA 7th Fluid and Plasma Dynamics Conference, Palo Alto, California, June 1-19, 1974.

12. Lewis, P. F. and Trainor, D. W. "Survey of Vibrational Relaxation Data for O_2, N_2, NO, H_2, CO, HF, HCl, CO_2, and H_2O." Report No. AMP 422, Avco Everett Research Laboratory, Everett, Massachusetts, November 1974.

13. Whitson, M. E., Jr. and McNeal, R. J. "Temperature Dependence of the Quenching of Vibrationally Excited N_2 by NO and H_2O." *Journal of Chemical Physics*, Vol. 66, No. 6, Mar 15, 1977, pp. 2696-2700.

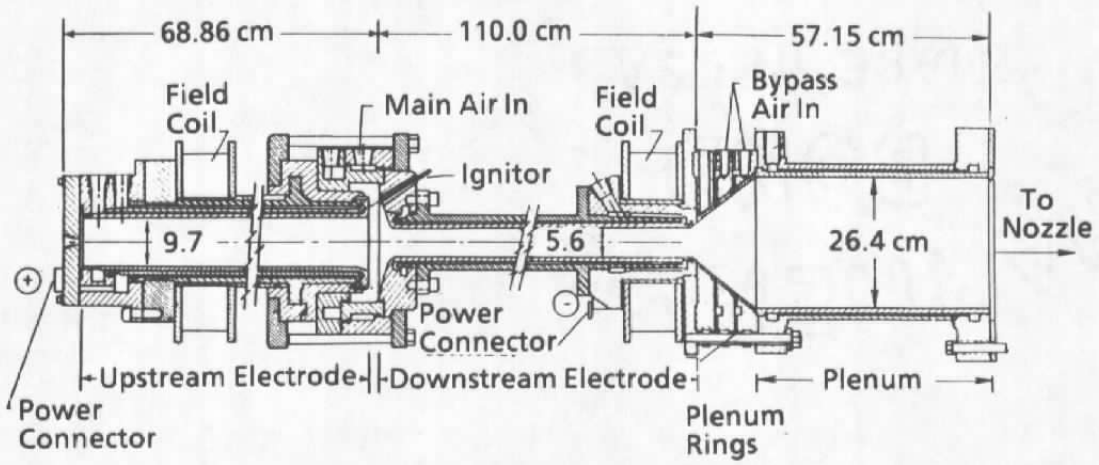

a. Arc heater and plenum chamber

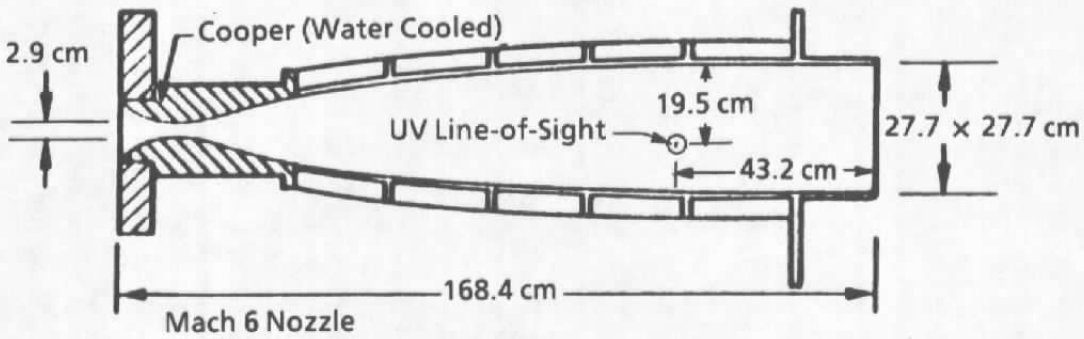

b. Mach 6 nozzle

Figure 1. Longitudinal section view of the NASA Langley Arc-Heated Scramjet Test Facility arc-heater, plenum chamber, and Mach 6 nozzle (Refs. 3, 4, and 5).

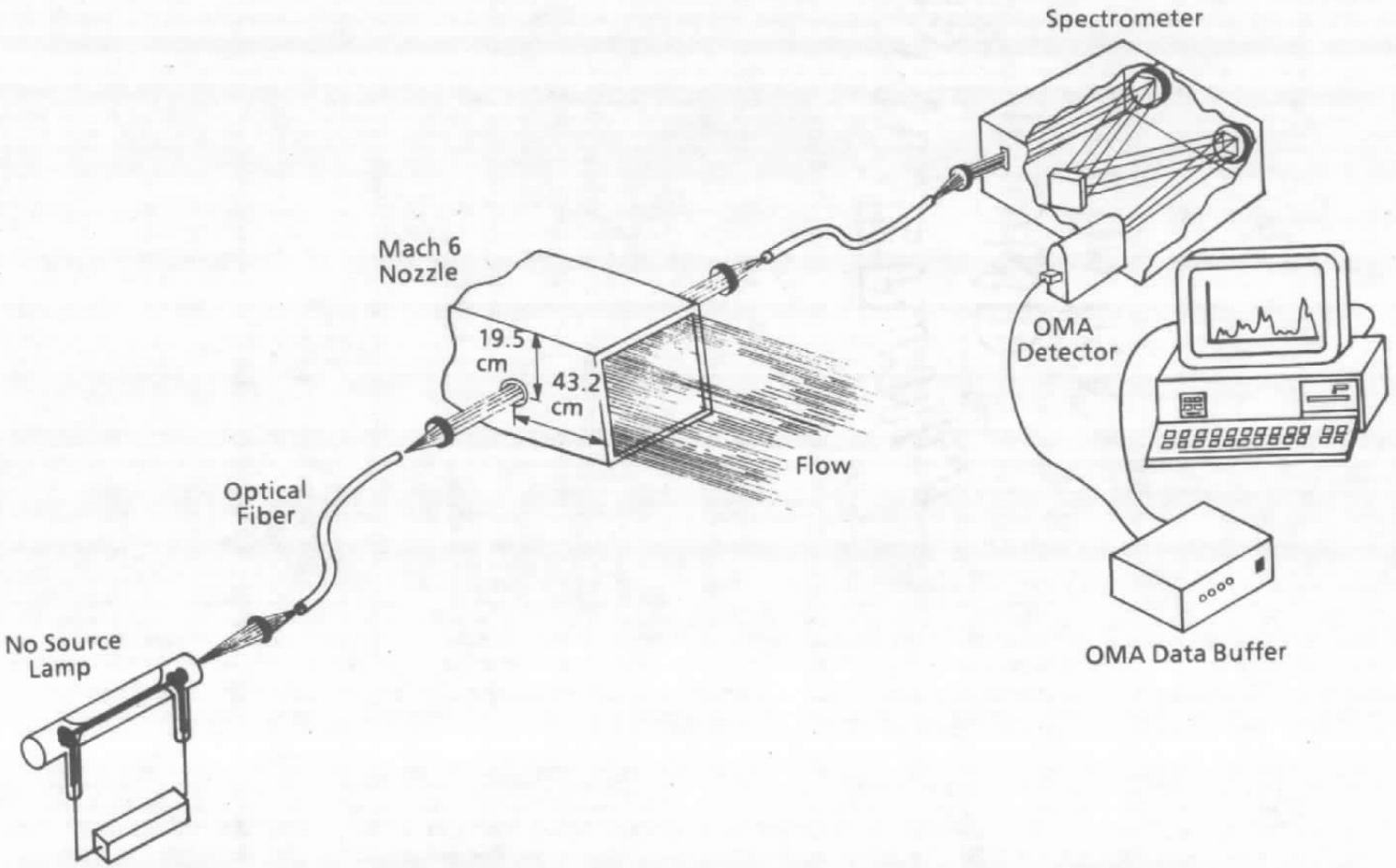

Figure 2. Illustration of the NO resonance absorption measurement system.

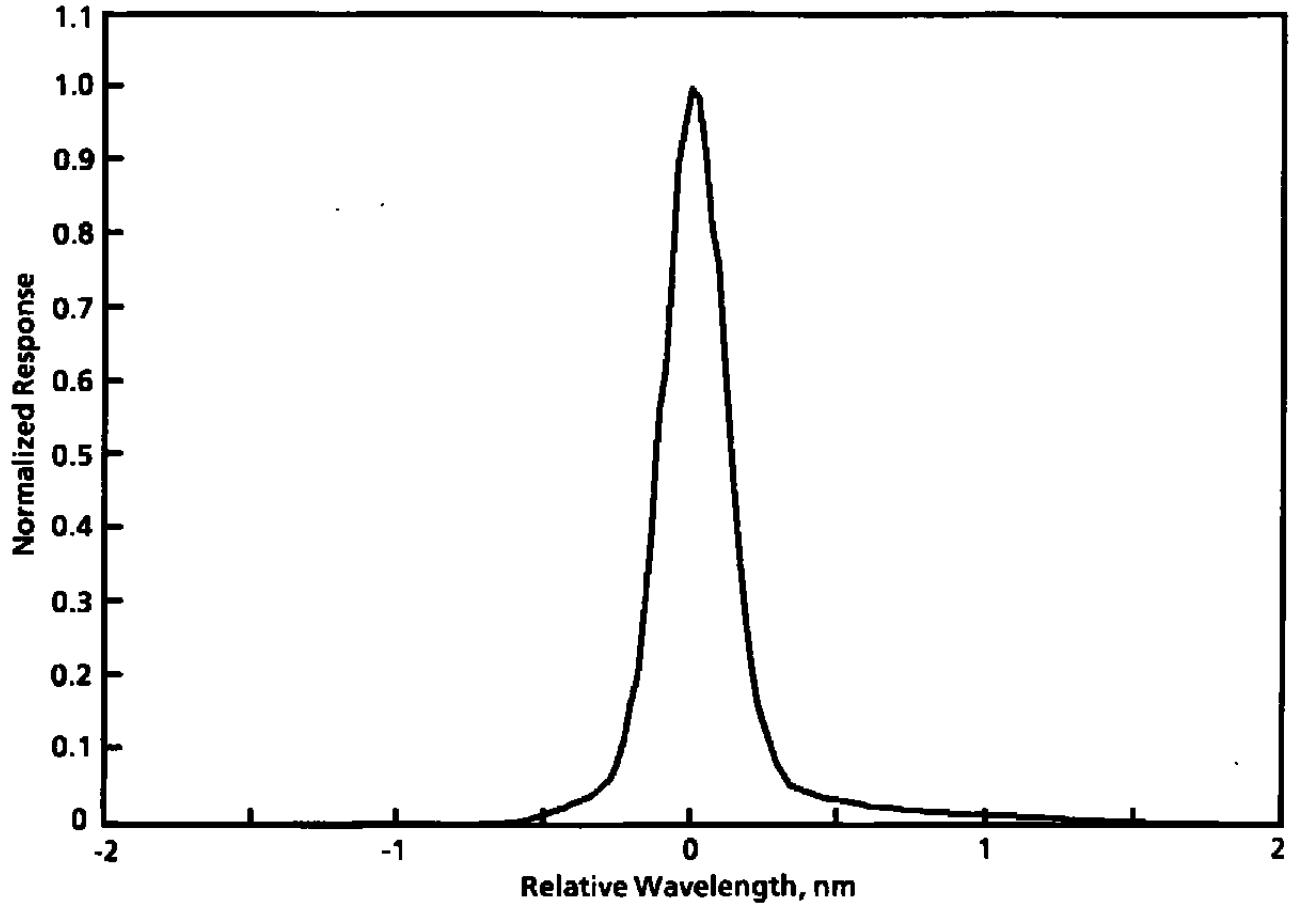

Figure 3. Instrument response function for the OMA Detector Element 39, the second bandhead of the (0,0) band.

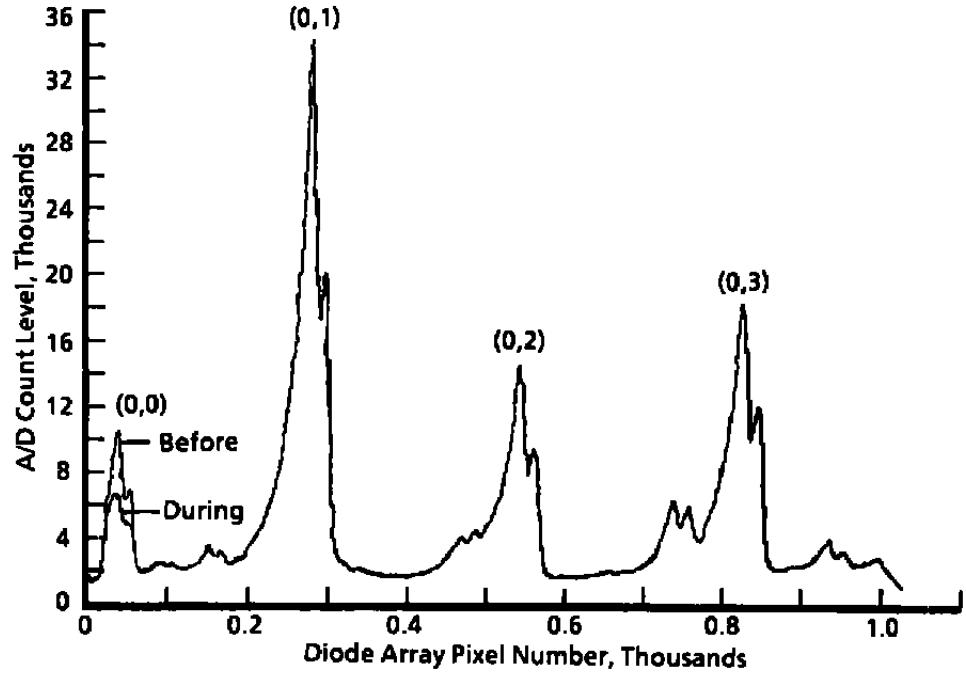

a. NO gamma bands within the detector bandpass

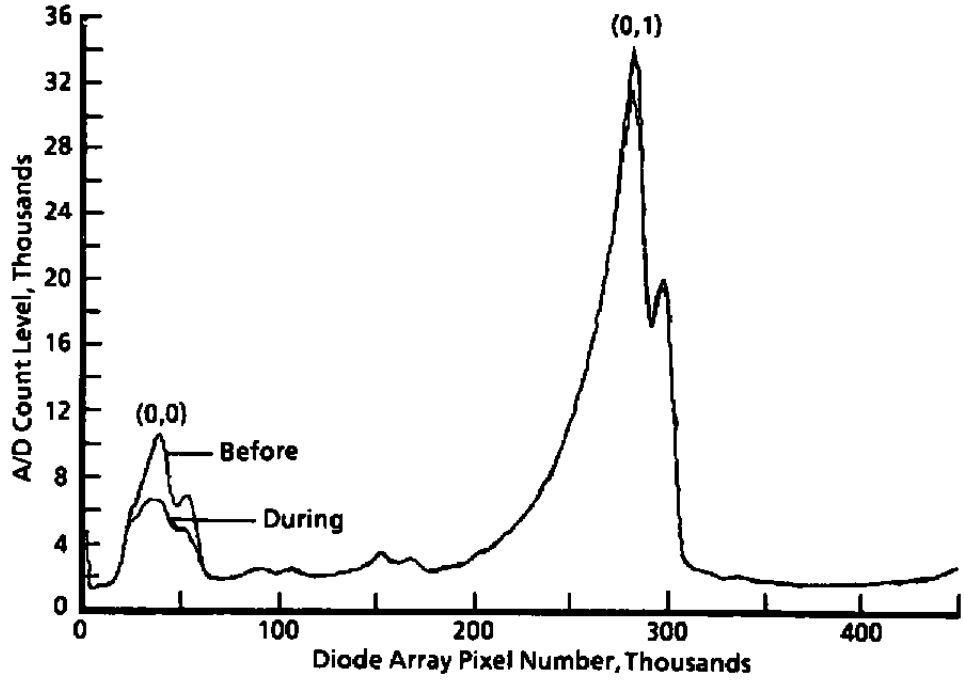

b. Detector pixels 1 to 450 of Fig. 4a

Figure 4. Typical lamp spectra before and during a test.

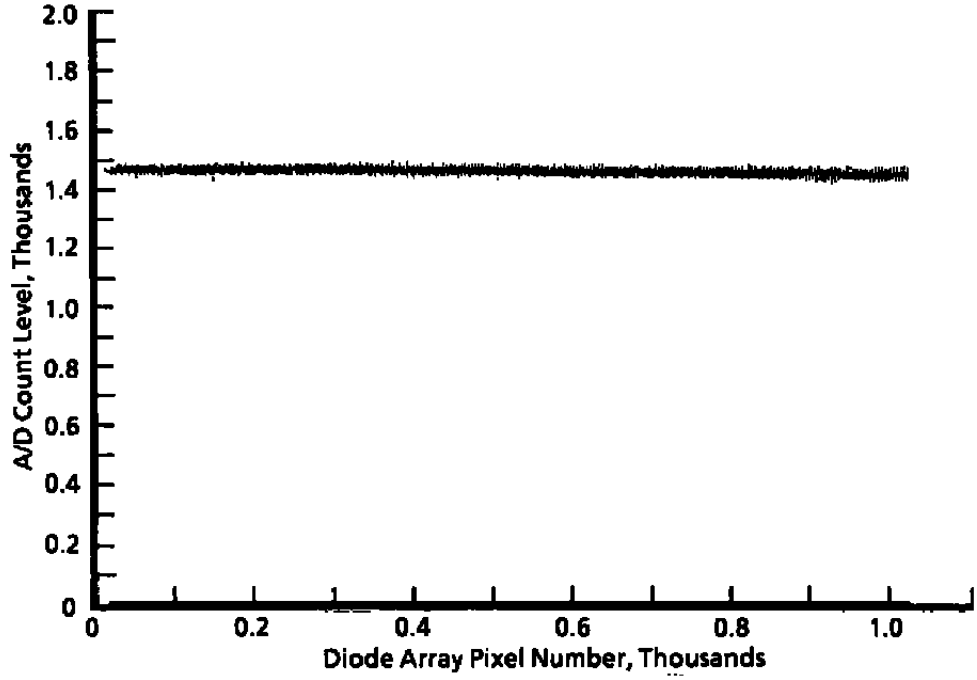

a. Pretest background scan

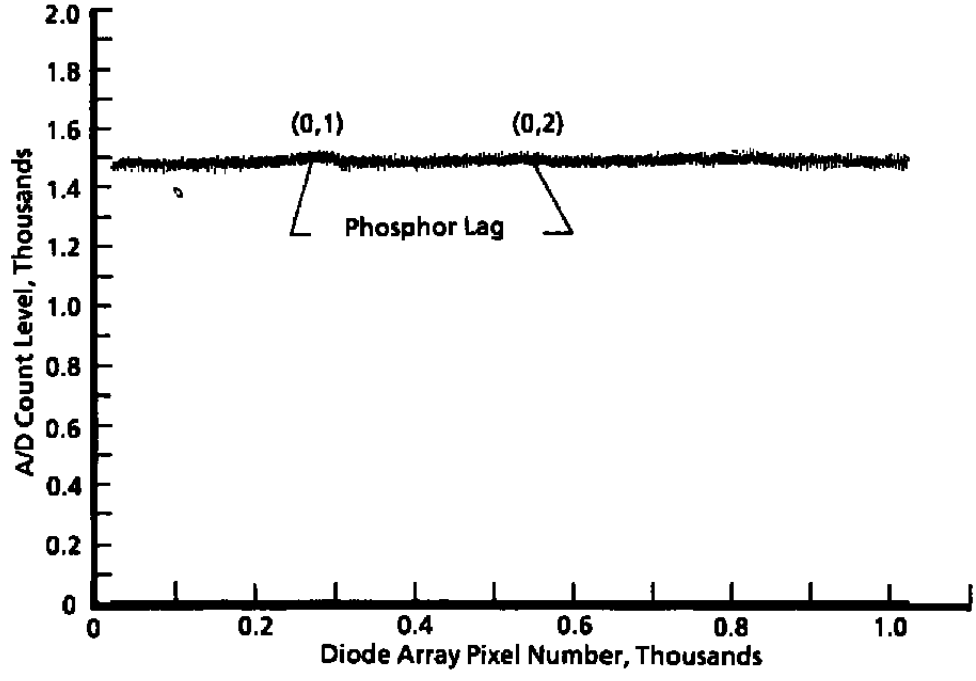

b. Flow-field emission plus background scan

Figure 5. Typical pretest detector background and flow-field emission plus background levels.

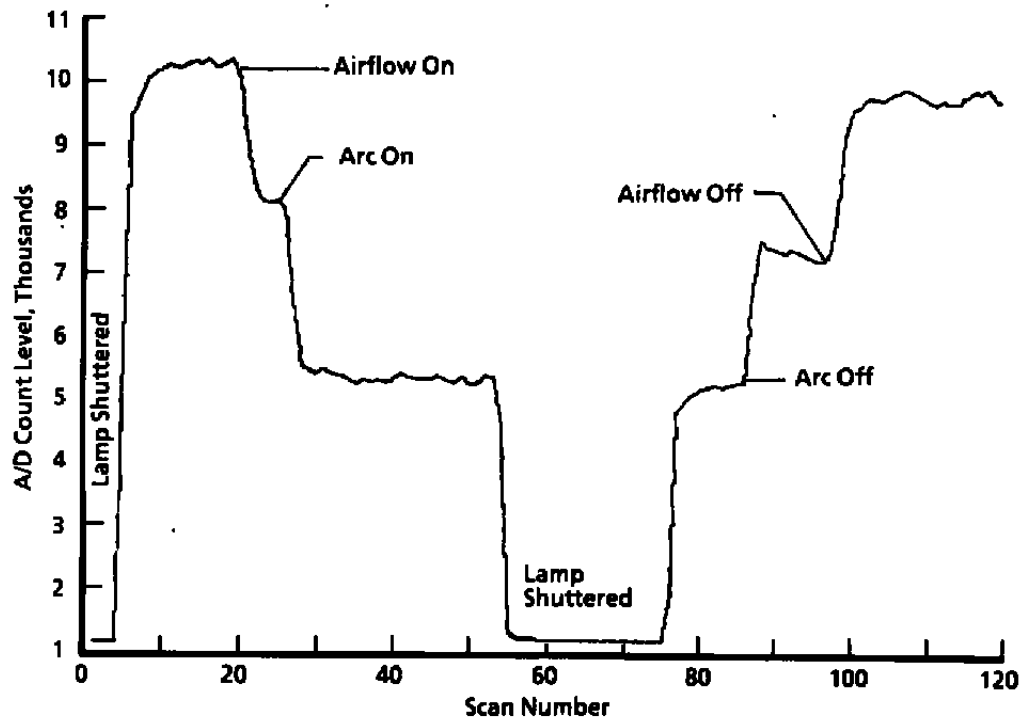

a. NO gamma (0,0) second bandhead signal level

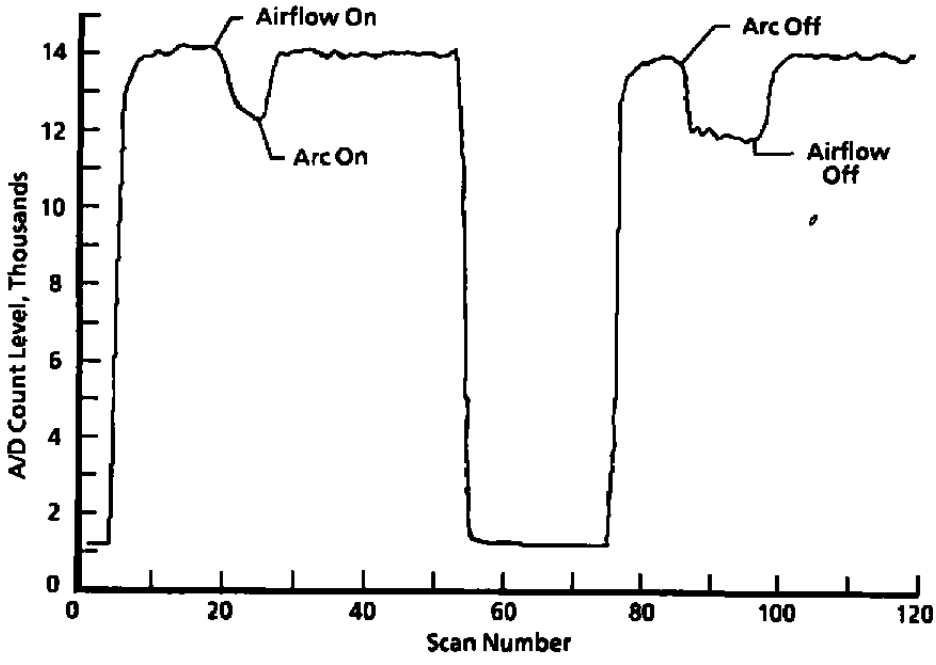

b. NO gamma (0,3) first bandhead signal level

Figure 6. Time history of the (0,0) and (0,3) band signal levels during Test R2B1; typical of the first nine tests described in Table 1.

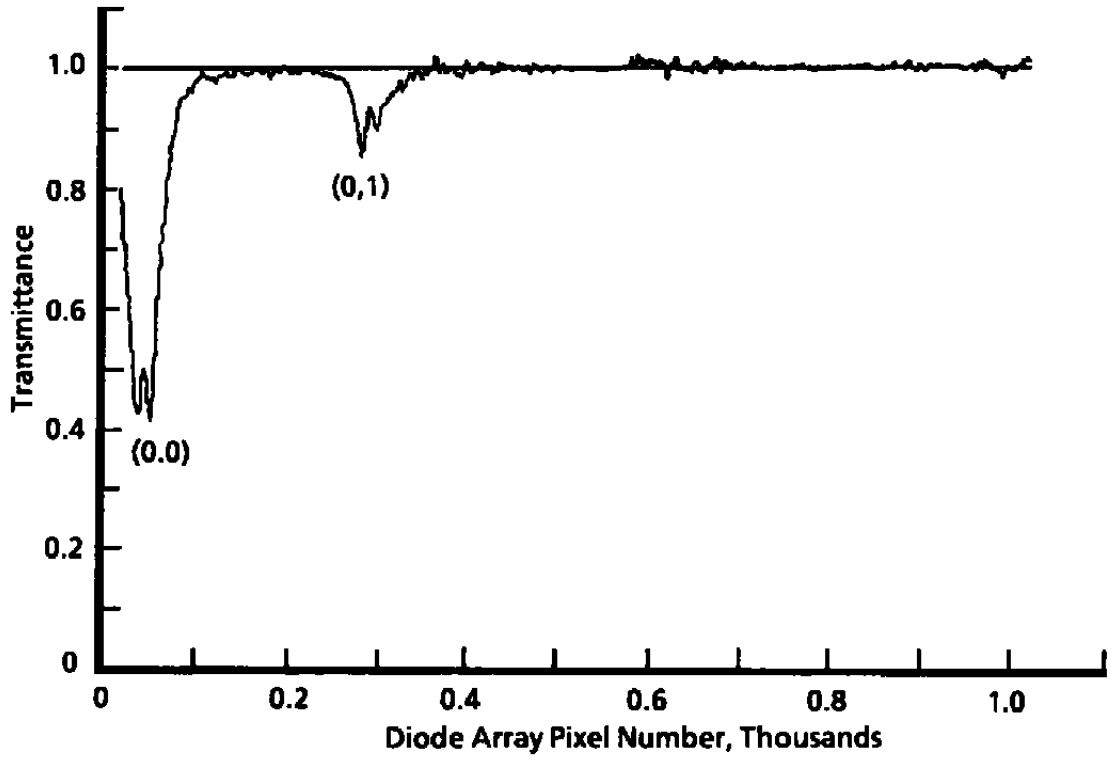

Figure 7. Transmittance data taken during Test R4B3; typical of the first tests described in Table 1.

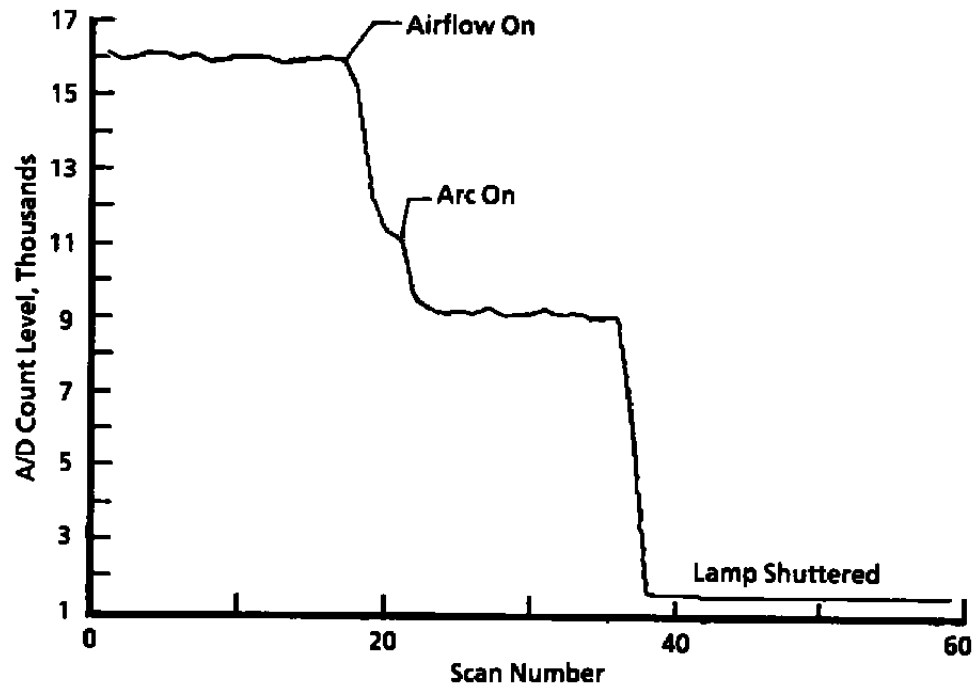

a. NO gamma (0,0) second bandhead signal level

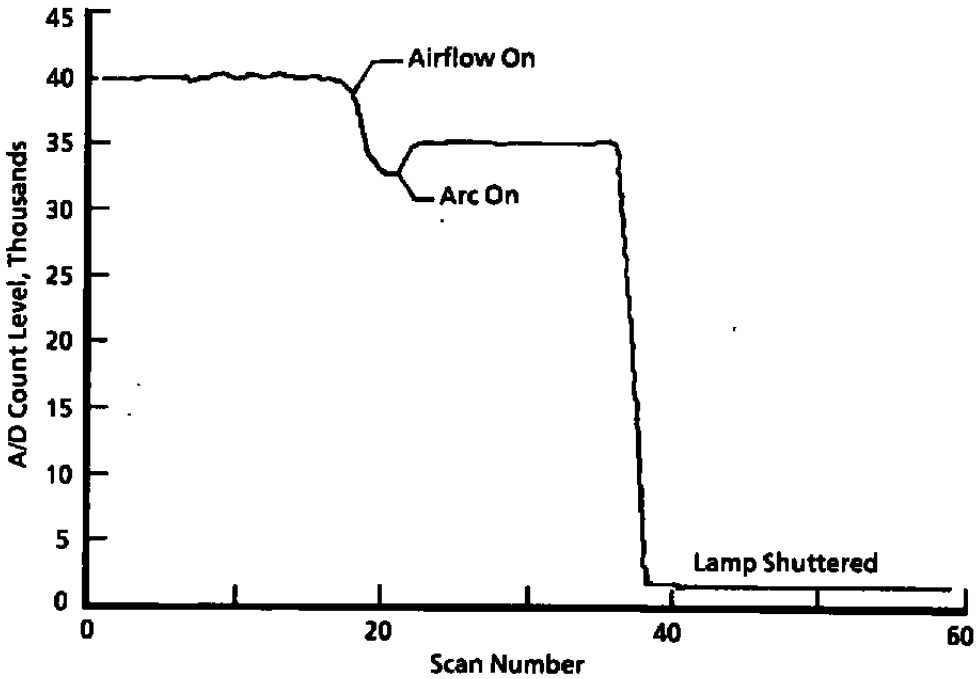

b. NO gamma (0,3) second bandhead signal level

Figure 8. Time history data of Test R4B4; typical of the last three tests described in Table 1.

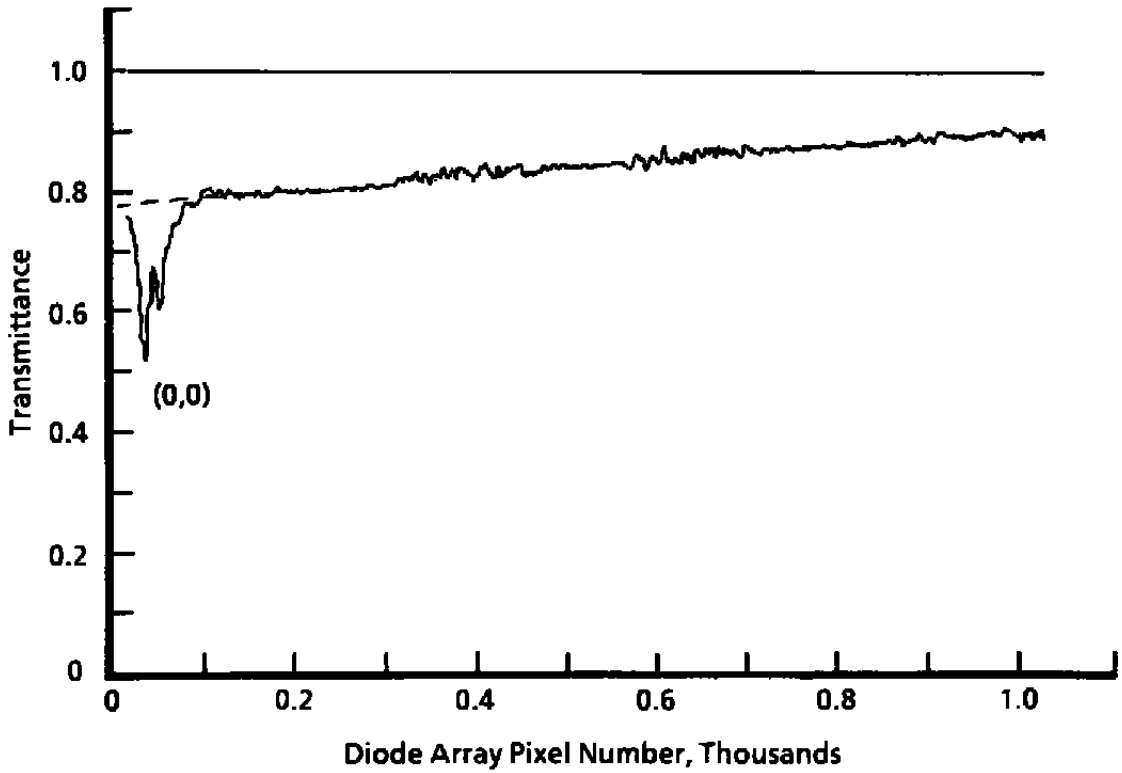

Figure 9. Transmittance data of Test R4B1; typical of the last three tests described in Table 1.

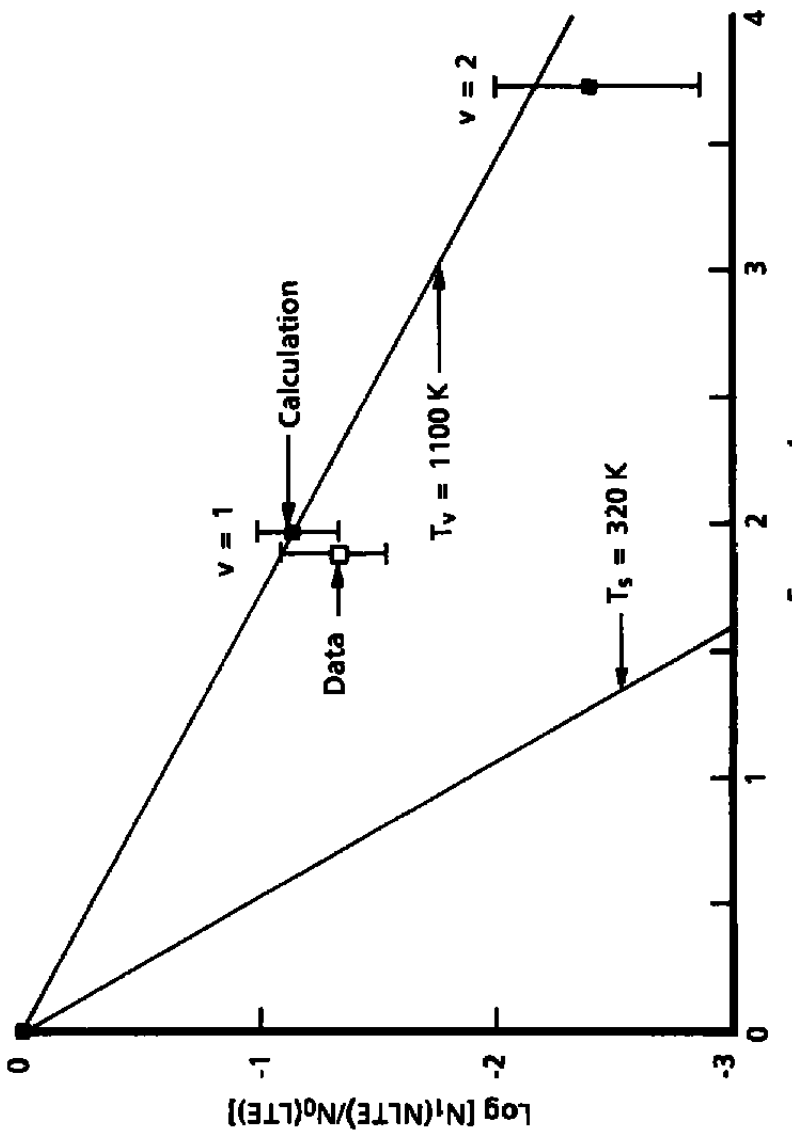

Figure 10. No relative Boltzmann plot, Test R3B4.

Table 1. NASA Langley Arc-Heated Scramjet Test Facility Parameters

Test	Main Air Flow, lb/sec	Bypass Air Flow, lb/sec	Total Air Flow, lb/sec	H_t btu/lbm	T_t, K	P_t, atm	T_s, K	P_s, atm
R1B1	0.52	1.3	1.82	735	1,556	9.32	187	4.70×10^{-3}
R2B1	1.13	3.4	4.53	750	1,578	24.50	189	12.25×10^{-3}
R2B2	1.475	4.455	6.025	730	1,544	31.30	186	15.65×10^{-3}
R3B1	0.52	0.68	1.2	1,027	2,322	7.28	279	3.67×10^{-3}
R3B2	1.13	2.0	3.13	950	1,944	18.71	223	9.39×10^{-3}
R3B3	1.59	2.92	4.51	990	2,000	27.42	240	13.75×10^{-3}
R3B4	1.13	1.07	2.18	1,400	2,667	15.11	320	7.55×10^{-3}
R4B2	1.59	2.92	4.51	980	1,986	26.95	238	13.47×10^{-3}
R4B3	1.59	2.92	4.51	1,020	2,056	27.35	247	13.68×10^{-3}
R2B3	0.52	4.46	4.98	325	736	18.30	88	9.19×10^{-3}
R4B1	0.52	4.46	4.98	325	725	18.16	87	9.12×10^{-3}
R4B4	0.52	4.46	4.98	320	725	18.16	87	9.12×10^{-3}

Table 2. Results of the NO Resonance Absorption Measurement

Test	τ (0,0) Measured	τ (0;1) Measured	NO Number Density, cm^{-3}	NO Mole Fraction	N_1, cm^{-3}	T_v, K
R1B1	0.58	0.93	2.83×10^{15}	0.015	5.1×10^{13}	671
R2B1	0.45	0.924	7.09×10^{15}	0.015	5.8×10^{13}	561
R2B2	0.43	0.935	7.78×10^{15}	0.013	4.9×10^{13}	533
R3B1	0.61	0.893	1.83×10^{15}	0.019	9.7×10^{13}	919
R3B2	0.48	0.85	5.06×10^{15}	0.016	1.4×10^{14}	750
R3B3	0.43	0.86	6.67×10^{15}	0.016	1.3×10^{14}	687
R3B4	0.54	0.87	2.67×10^{15}	0.015	1.3×10^{14}	899
R4B2	0.43	0.86	6.75×10^{15}	0.016	1.3×10^{14}	684
R4B3	0.43	0.86	6.52×10^{15}	0.016	1.3×10^{14}	693
R2B3	0.64	1.0	1.97×10^{15}	0.0026	—	—
R4B1	0.69	1.0	1.29×10^{15}	0.0017	—	—
R4B4	0.69	1.0	1.29×10^{15}	0.0017	—	—

APPENDIX A

INTENSIFIED SILICON PHOTODIODE ARRAY DETECTOR

The detector used in this work is shown schematically in Fig. A-1. For a more complete and detailed description, the reader is referred to the EG&G Princeton Applied Research Corporation (Ref. A-1). The detector is placed so that the detector focal plane and the exit focal plane of the spectrometer are coincident. Photons striking the photocathode release electrons that are accelerated into the microchannel plate (MCP) consisting of a bundle of fine glass tubes having partially conductive walls. The microchannels act as electron multipliers. Electrons that exit the MCP are accelerated to the phosphor screen causing it to emit photons that are transmitted through fiber optics to a linear 1,024-element silicon photodiode array.

REFERENCE

A-1. EG&G Princeton Applied Research Product Literature. "Models 1420 and 1421 Solid-State Detectors Instruction Manual." Princeton Applied Research Corporation, 1988.

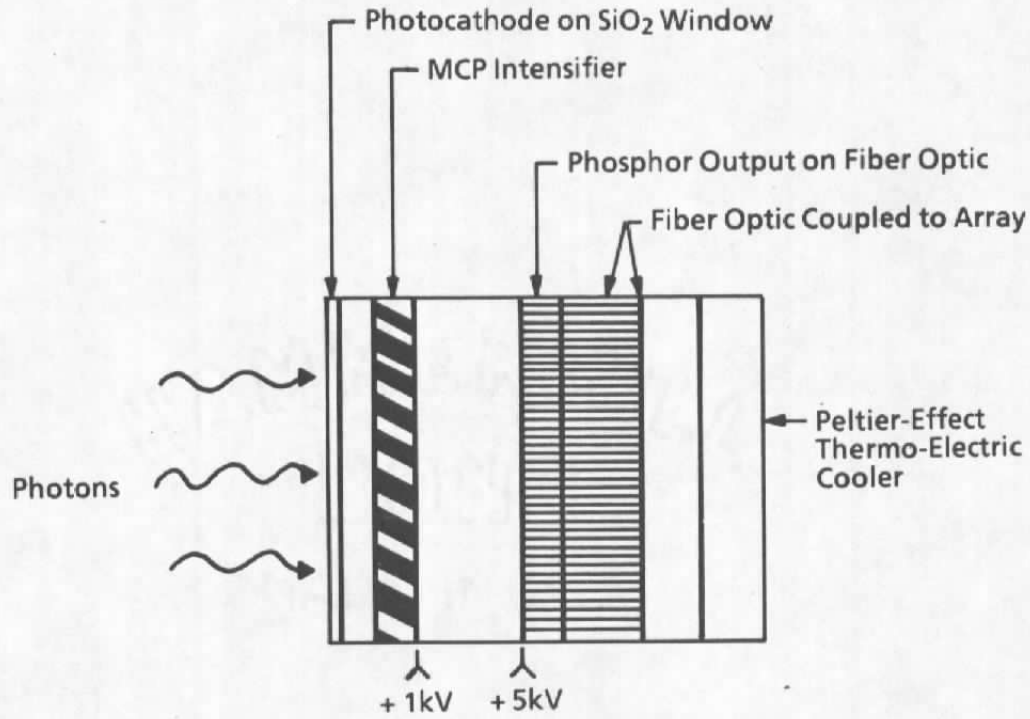

Figure A-1. Illustration of the proximity focused multichannel plate (MCP) intensifier coupled to the silicon photodiode array.

APPENDIX B

SUMMARY OF TEST DATA

Data acquired on the 12 tests conducted at the NASA Langley Arc-Heated Scramjet Engine Test Facility using the NO resonance absorption system instrumentation are presented in Figs. B-1 through B-12. Each figure contains a typical plot of spectral transmittance and a time history plot of the transmittance of both the NO gamma (0,0) and (0,3) second bandheads versus scan number (time) throughout the test. The spectral transmittance plots have not been adjusted to a transmittance value of 100 percent outside the absorbing NO bands as discussed in this report. Thus, the values in the plots may deviate from the transmittance values listed in Table 2.

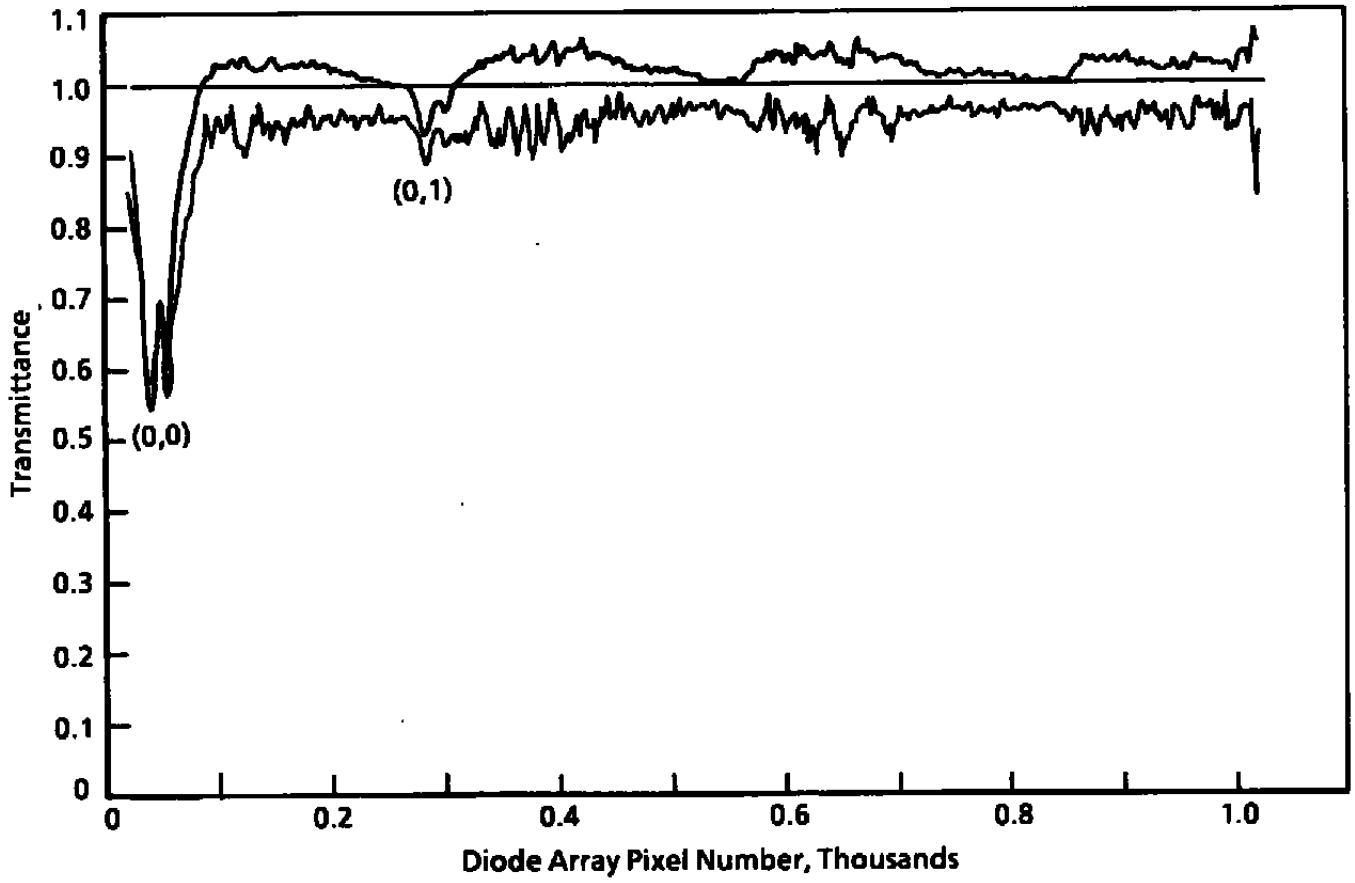

a. Spectral transmittance

Figure B-1. Spectral transmittance and a time history of the NO gamma (0,0) and (0,3) band transmittances for Test R1B1.

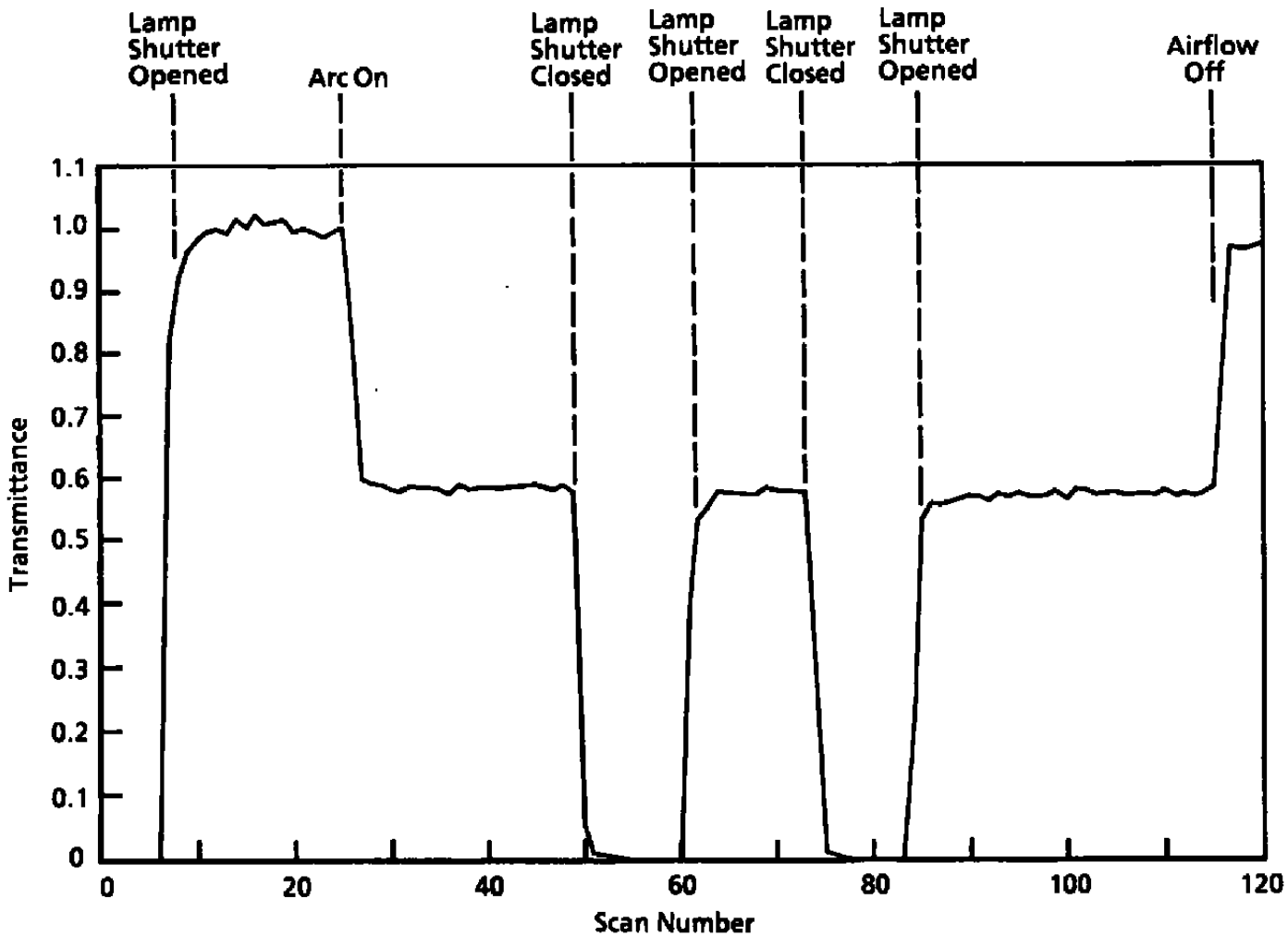

b. NO gamma (0,0) second bandhead transmittance
Figure B-1. Continued.

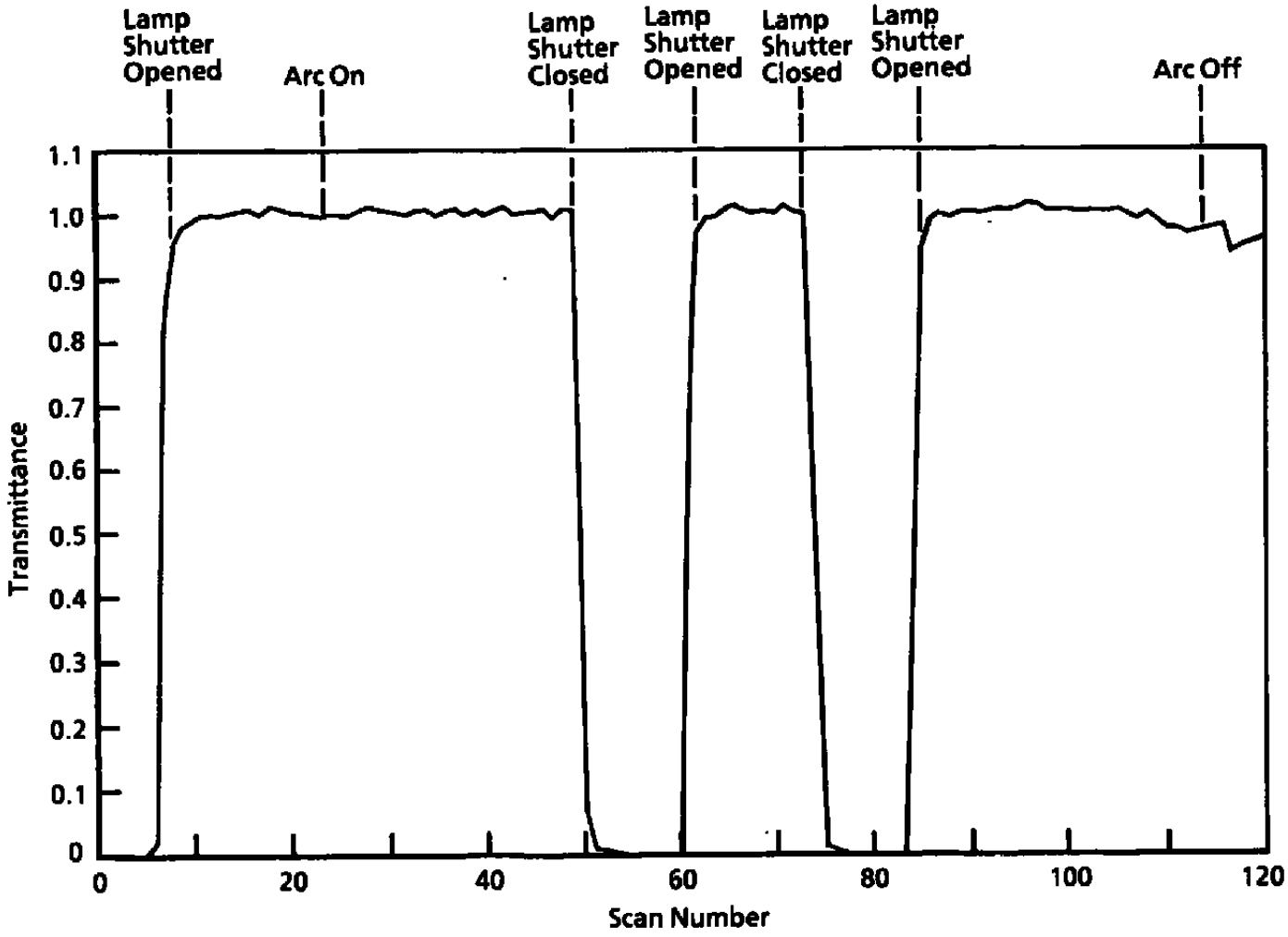

c. NO gamma (0,3) second bandhead transmittance

Figure B-1. Concluded.

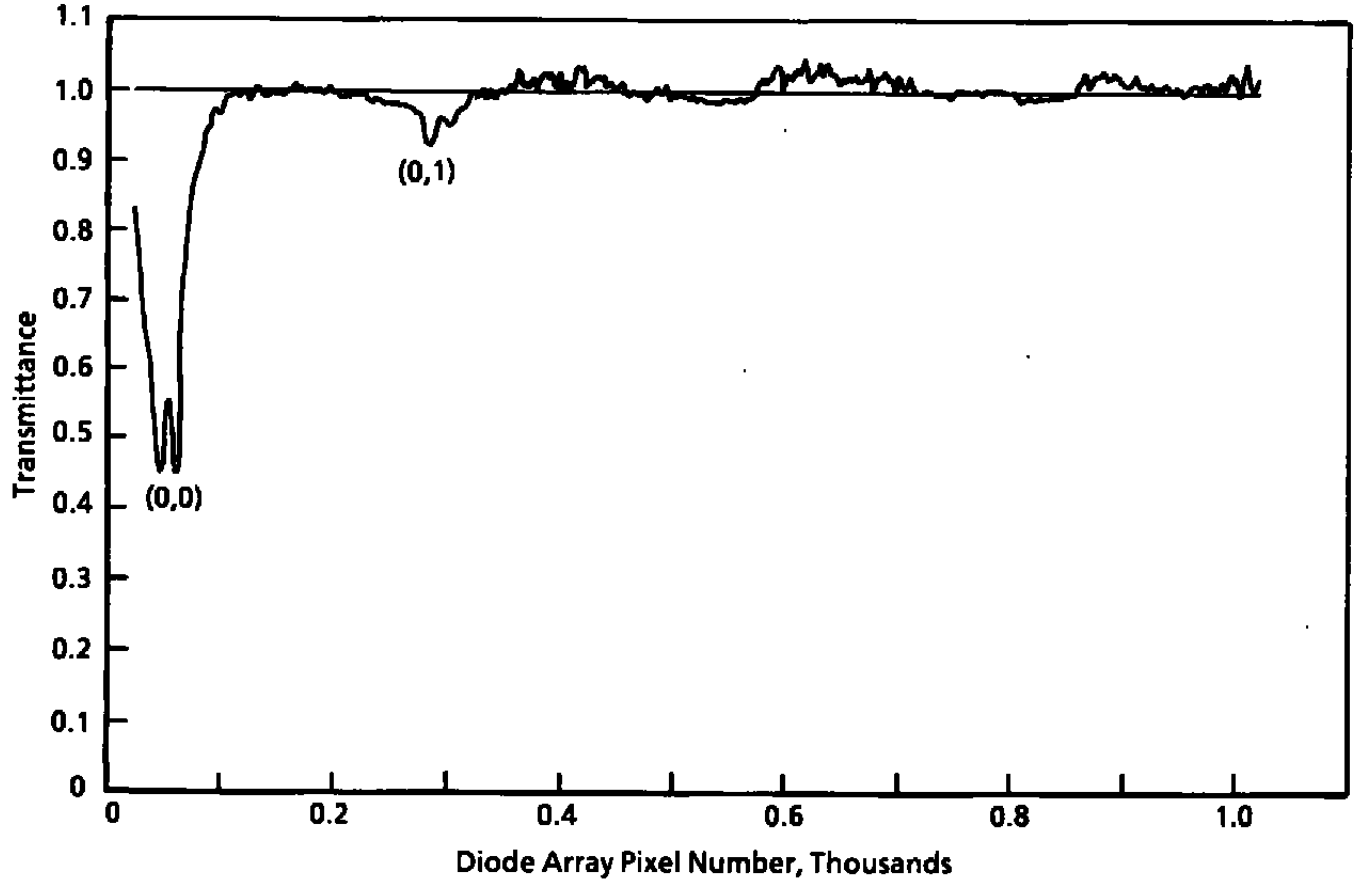

a. Spectral transmittance

Figure B-2. Spectral transmittance and a time history of the NO gamma (0,0)and (0,3) band transmittances for Test R2B1.

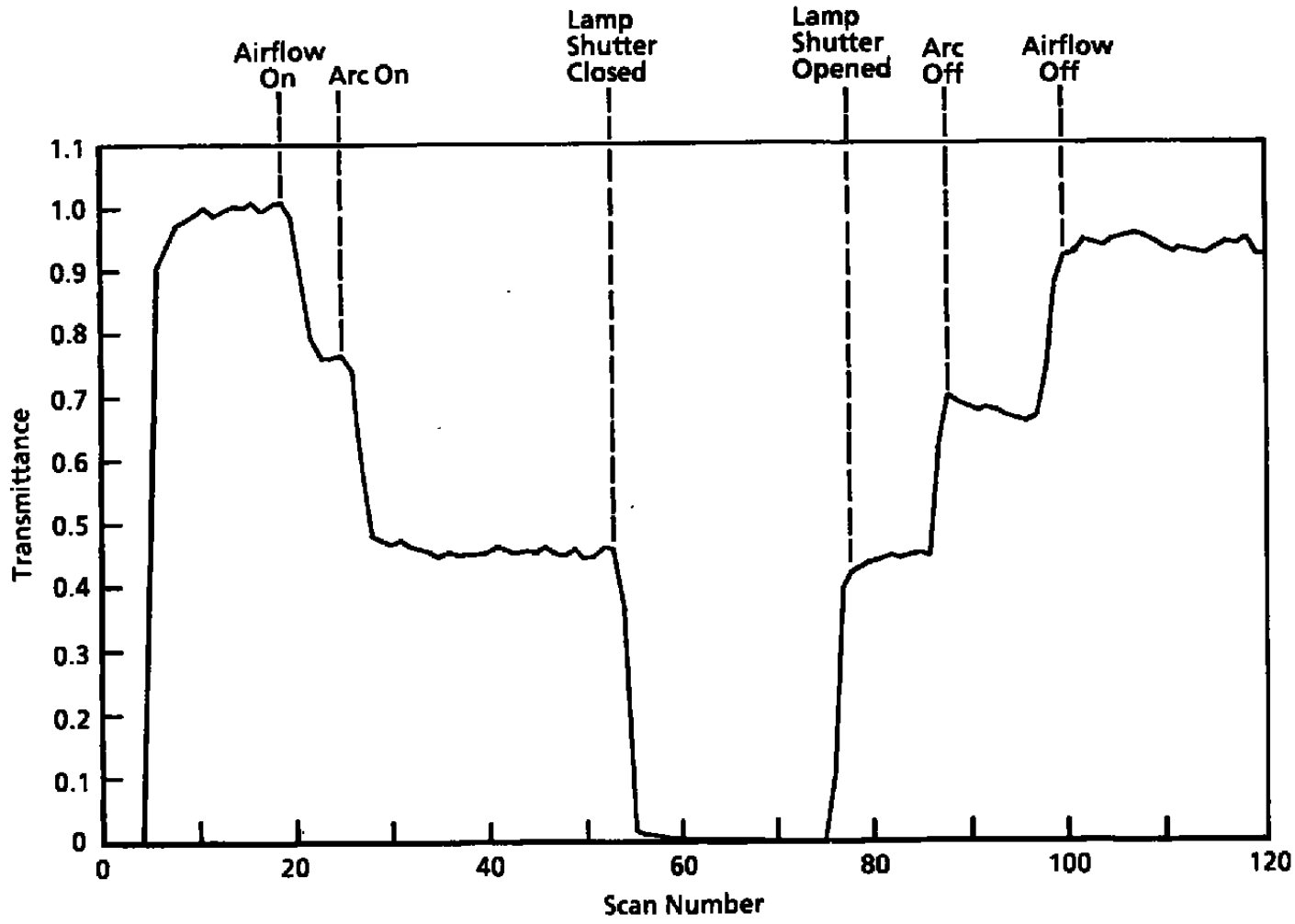

b. NO gamma (0,0) second bandhead transmittance
Figure B-2. Continued.

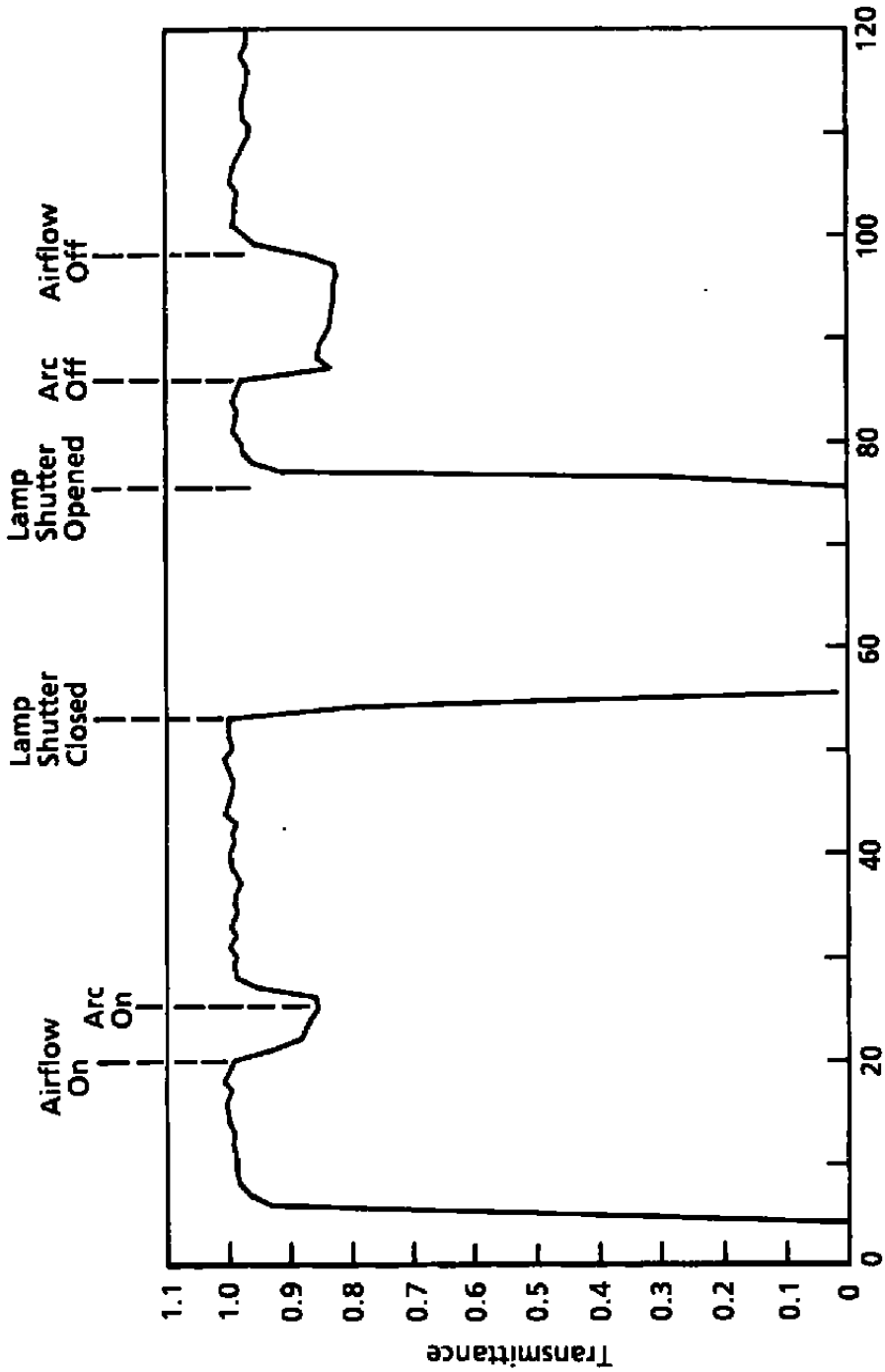

c. No gamma (0,3) second bandhead transmittance

Figure B-2. Concluded.

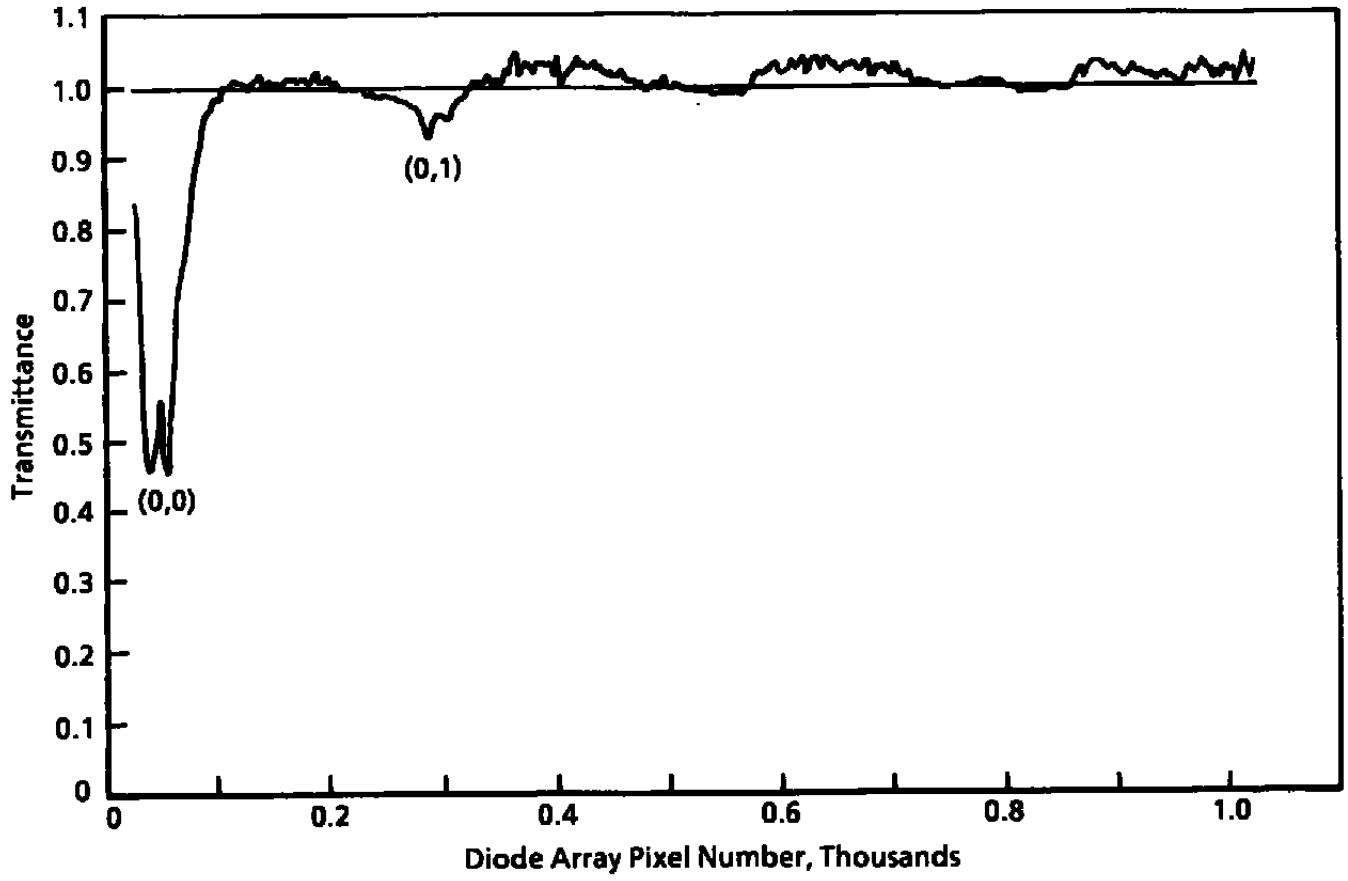

a. Spectral transmittance

Figure B-3. Spectral transmittance and a time history of the NO gamma (0,0)and (0,3) band transmittances for Test R2B2.

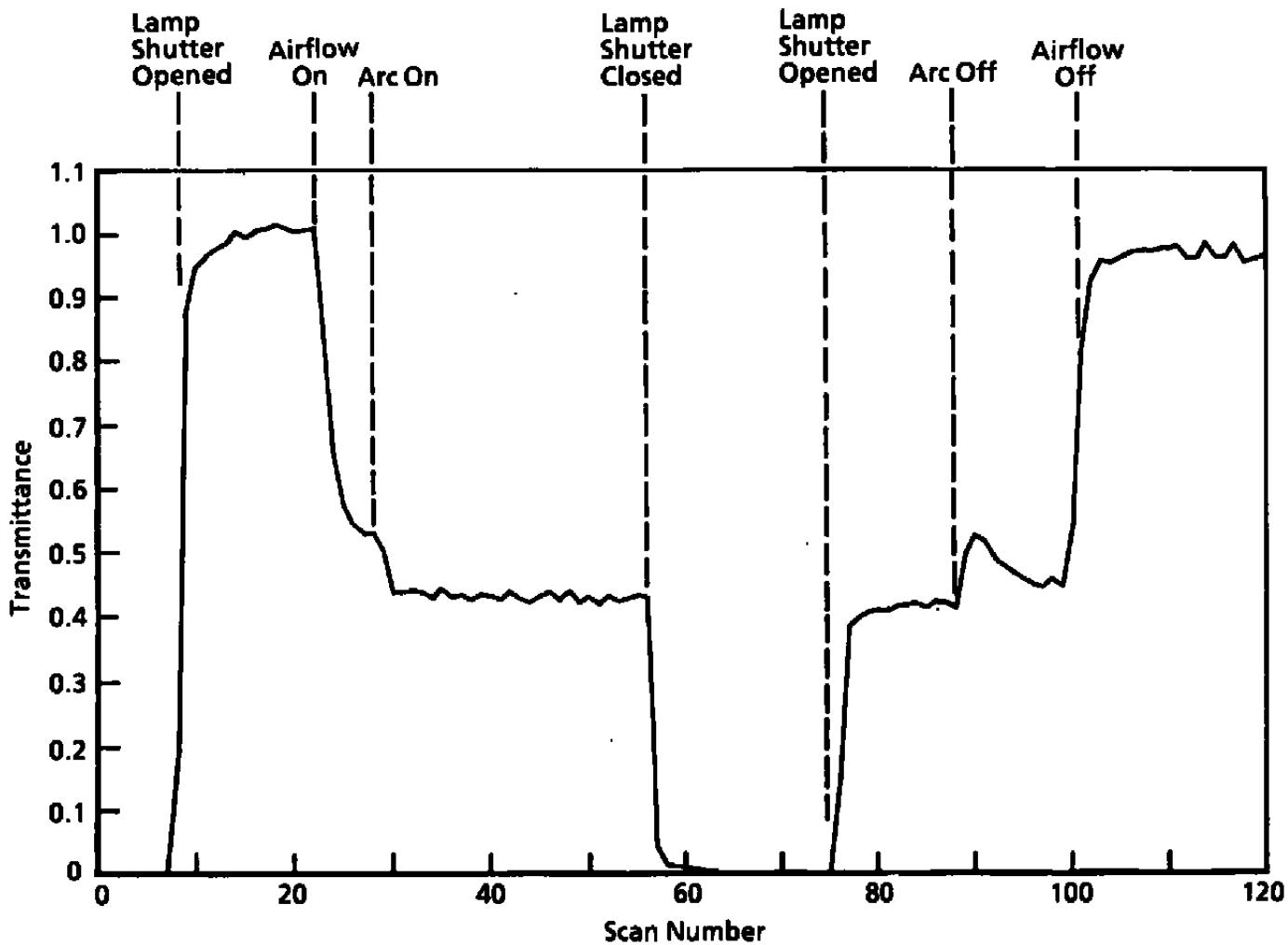

b. NO gamma (0,0) second bandhead transmittance
Figure B-3. Continued.

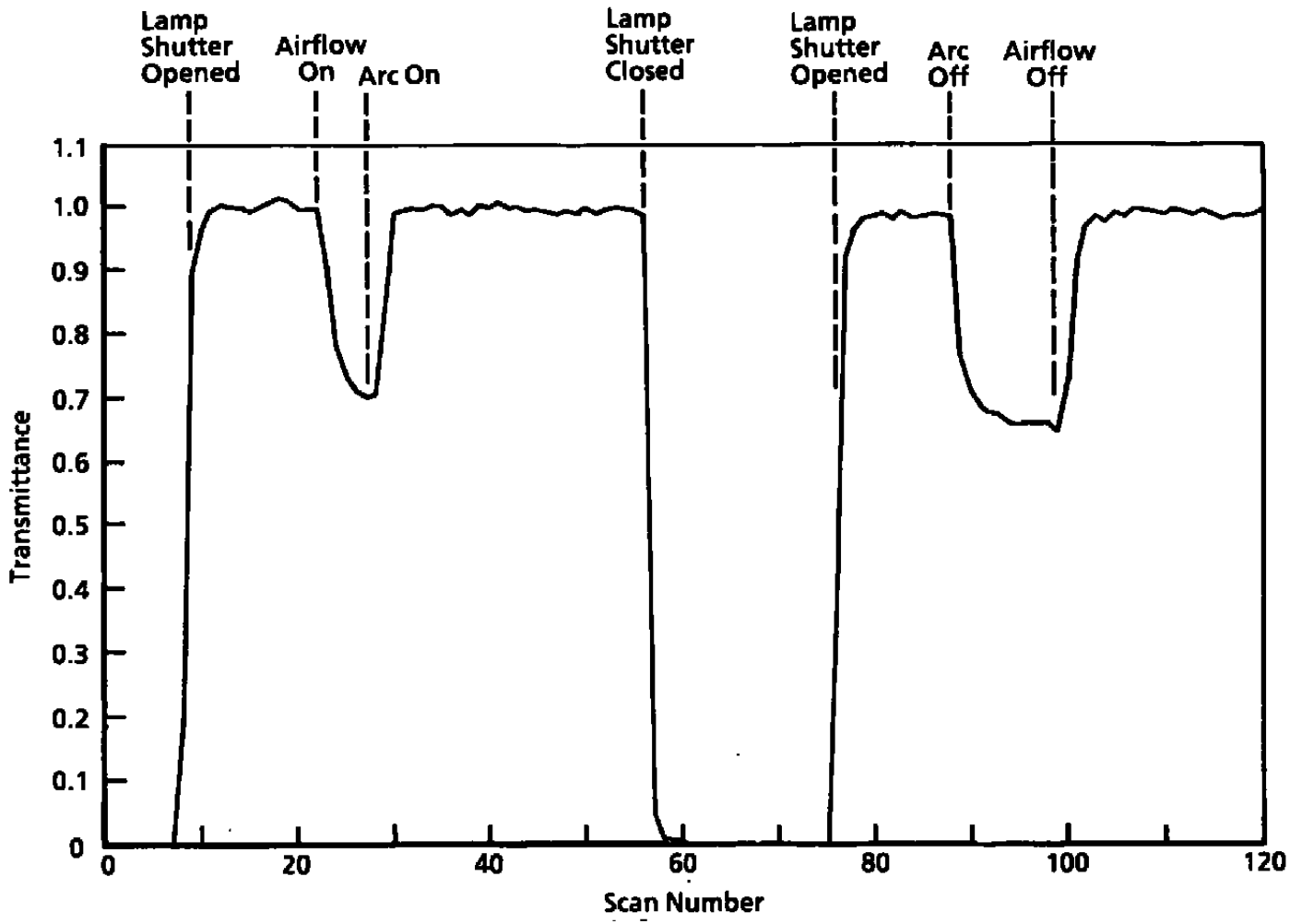

c. No gamma (0,3) second bandhead transmittance

Figure B-3. Concluded.

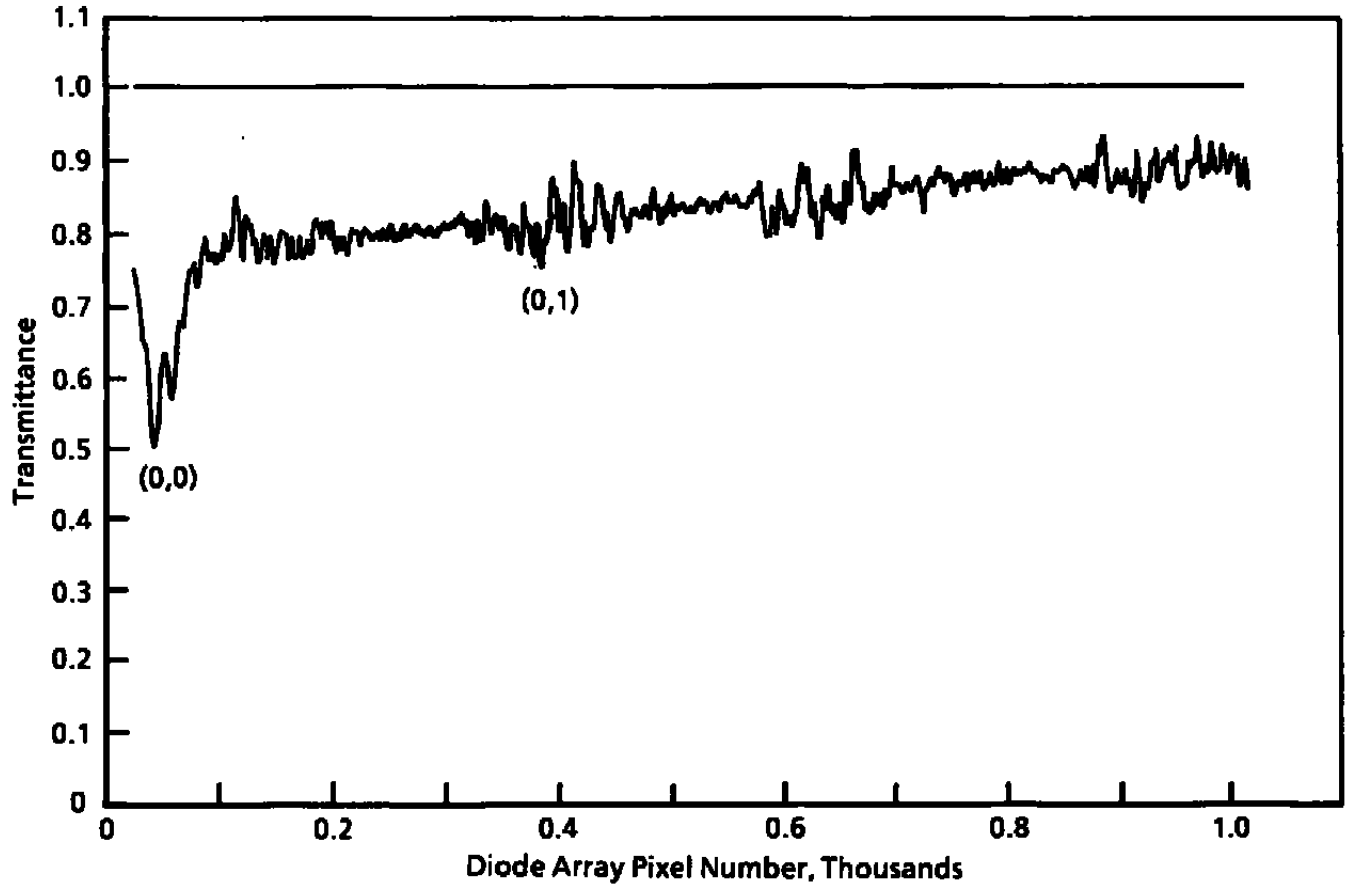

a. Spectral transmittance

Figure B-4. Spectral transmittance and a time history of the NO gamma (0,0)and (0,3) band transmittances for Test R2B3.

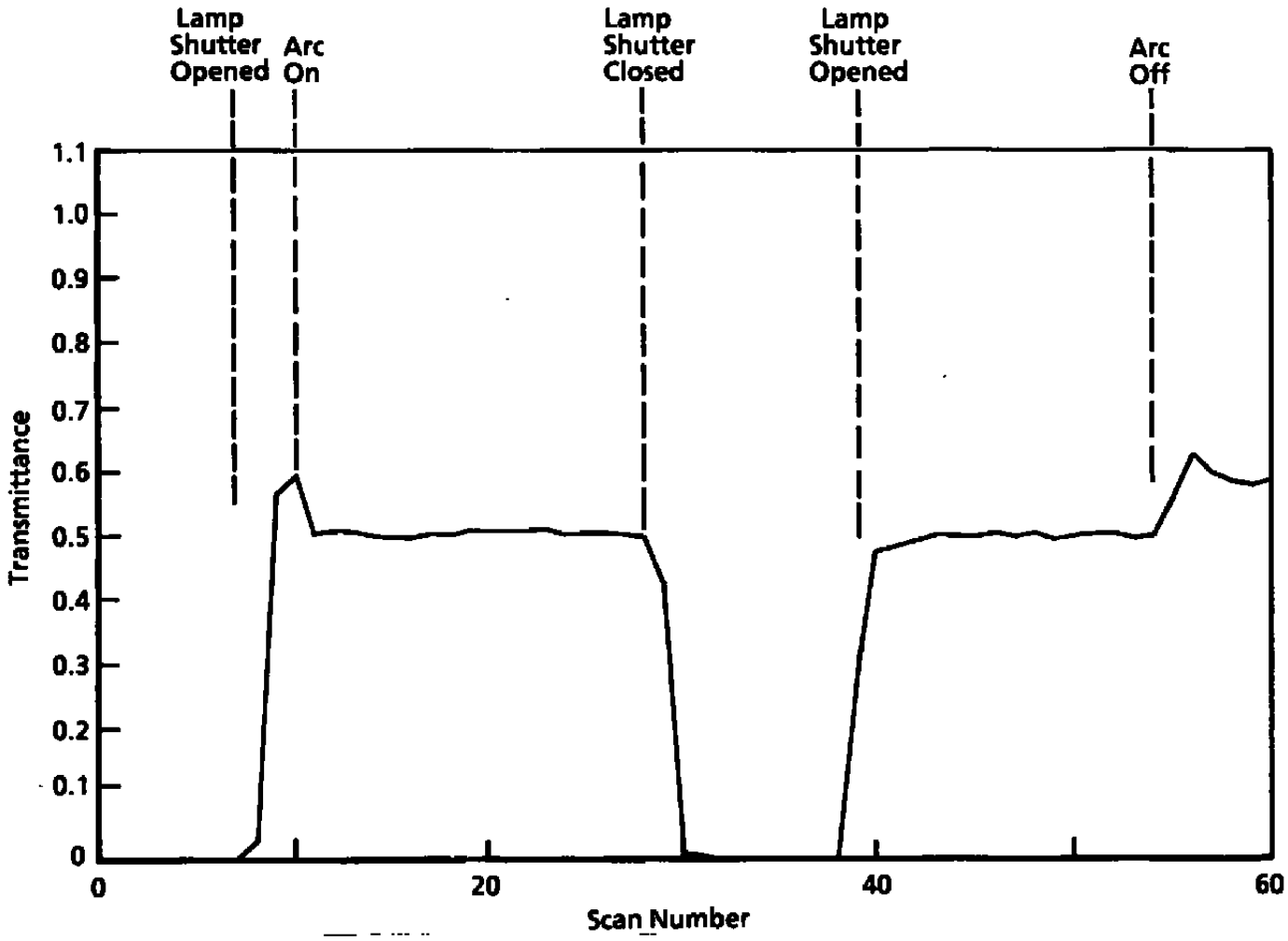

b. NO gamma (0,0) second bandhead transmittance
Figure B-4. Continued.

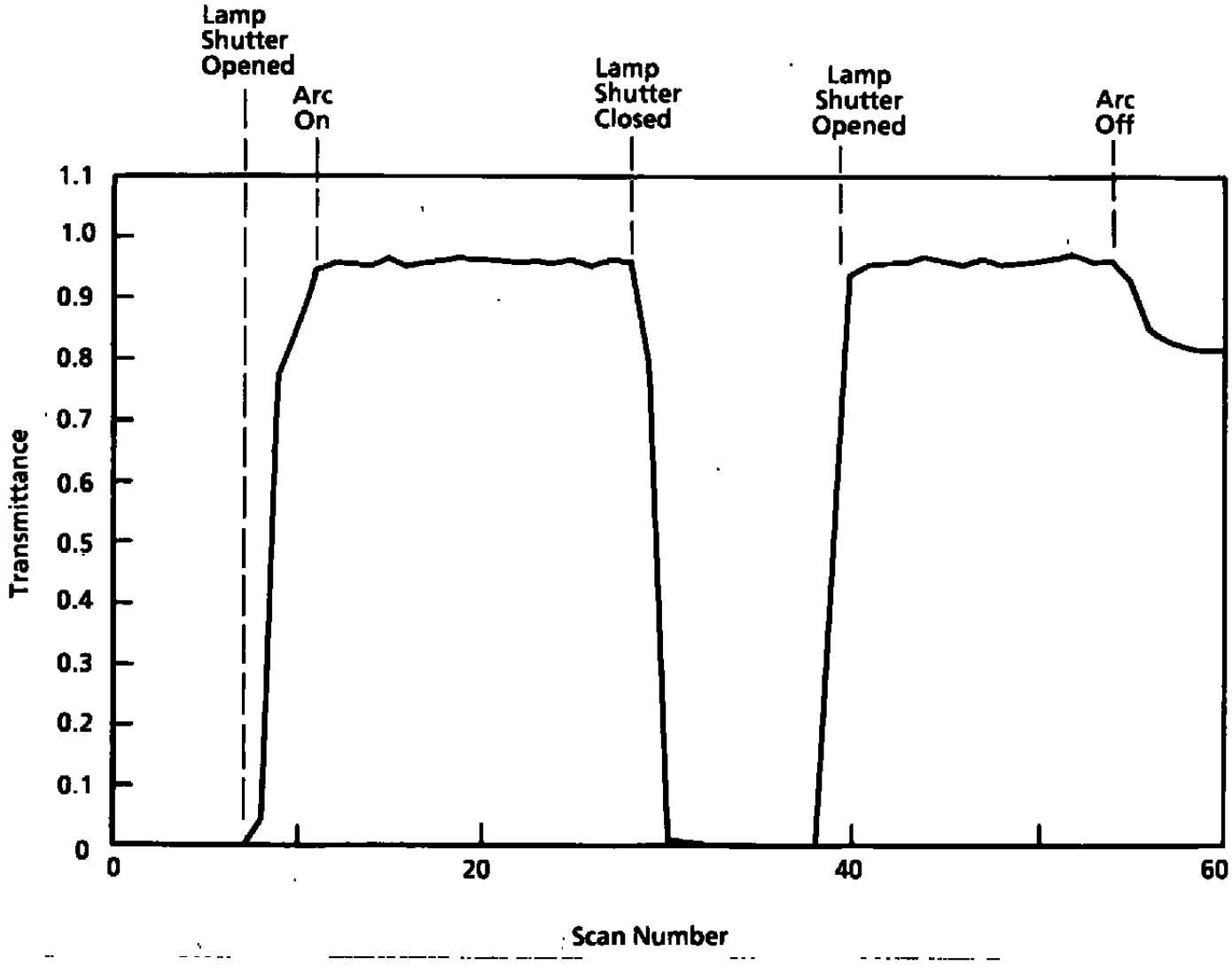

c. No gamma (0,3) second bandhead transmittance

Figure B-4. Concluded.

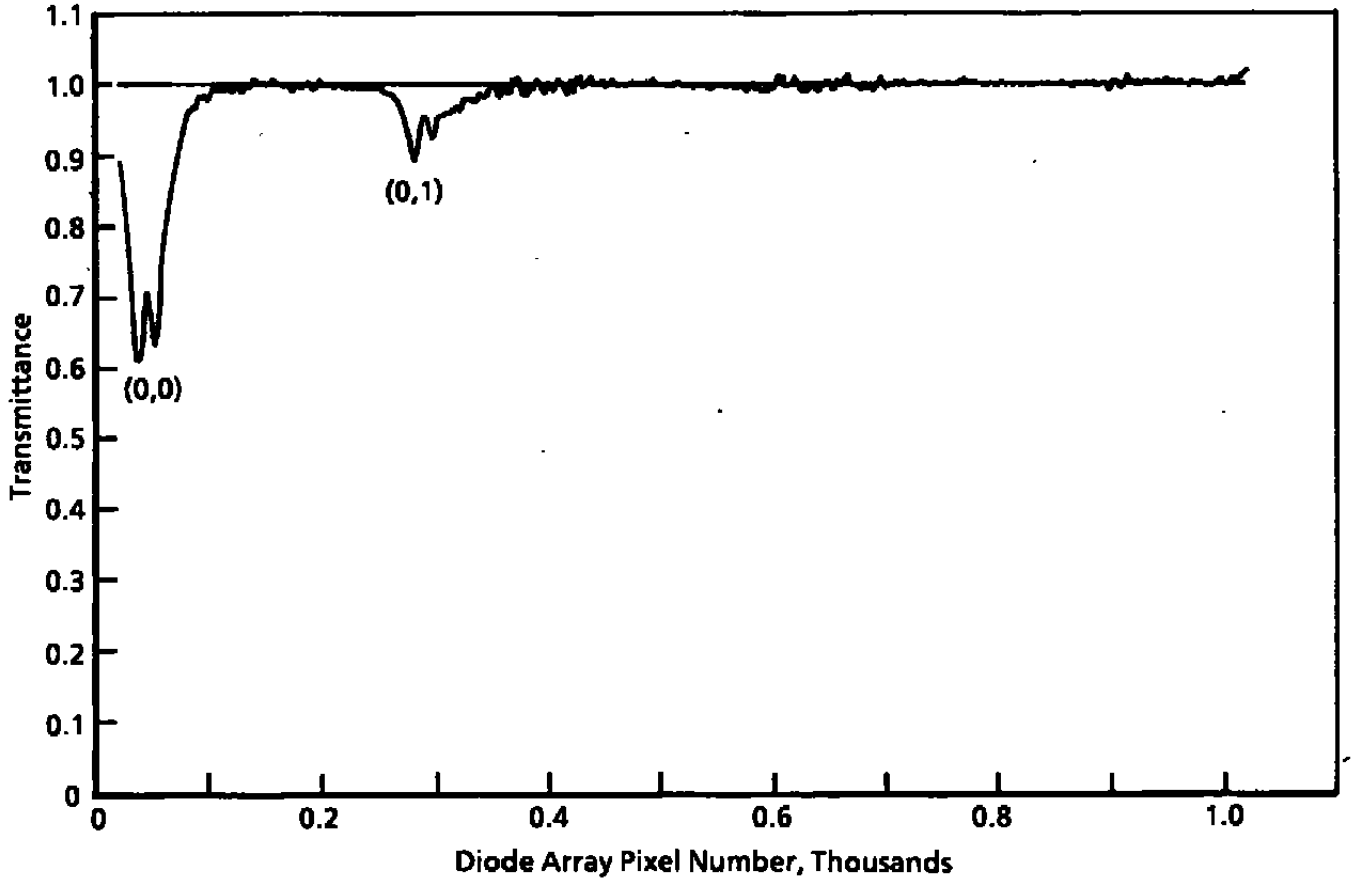

a. Spectral transmittance

Figure B-5. Spectral transmittance and a time history of the NO gamma (0,0)and (0,3) band transmittances for Test R3B1.

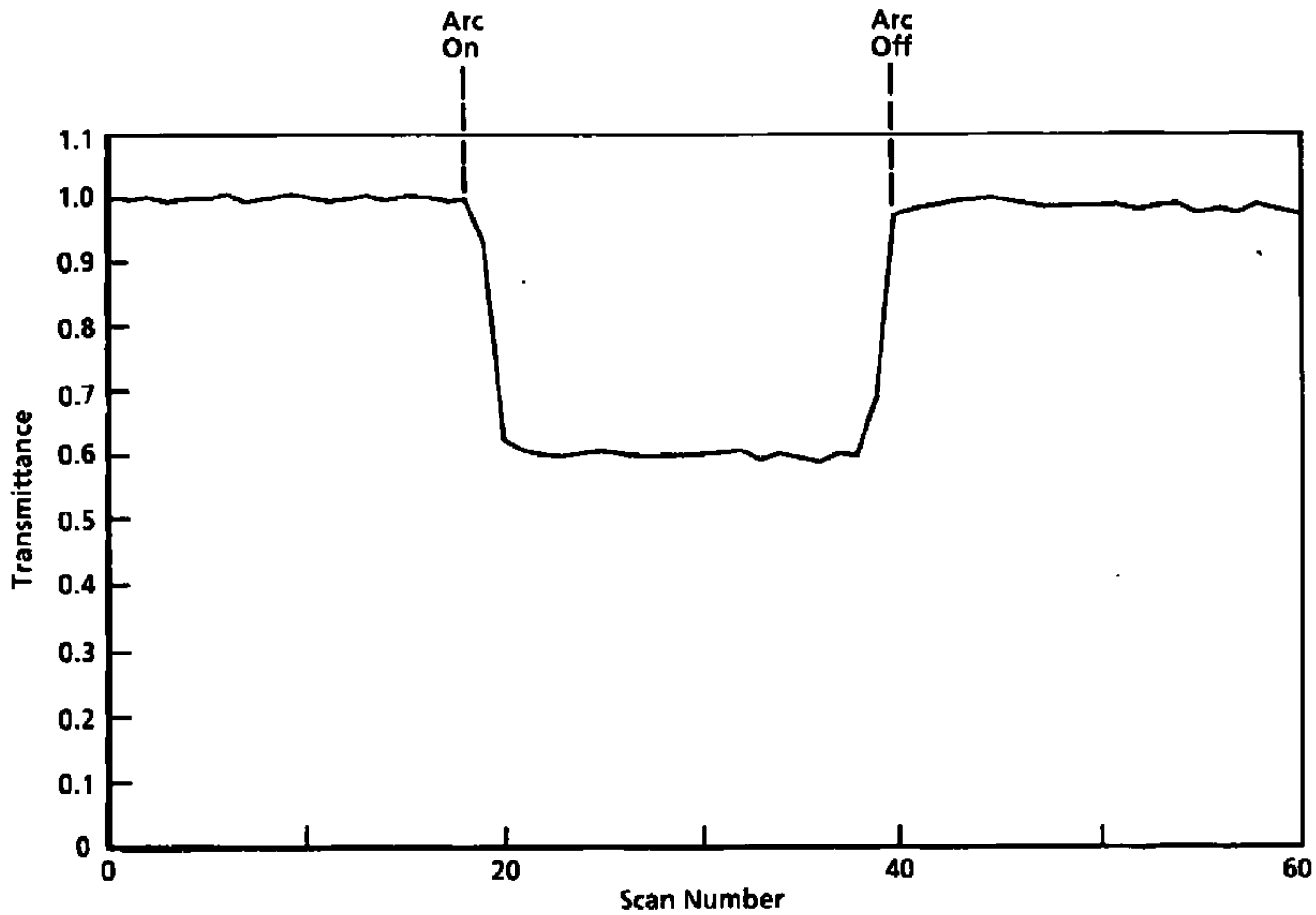

b. NO gamma (0,0) second bandhead transmittance
Figure B-5. Continued.

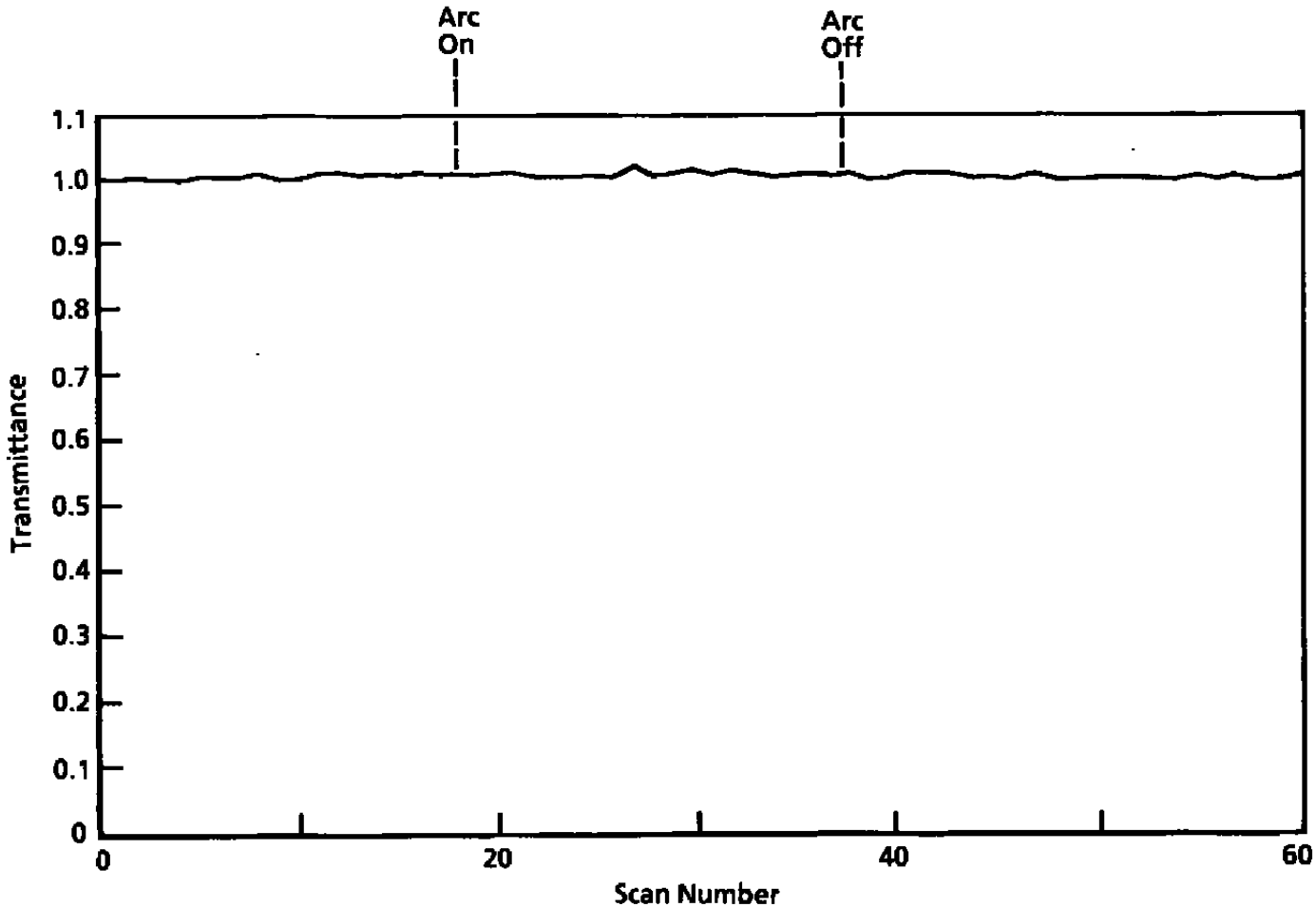

c. No gamma (0,3) second bandhead transmittance
Figure B-5. Concluded.

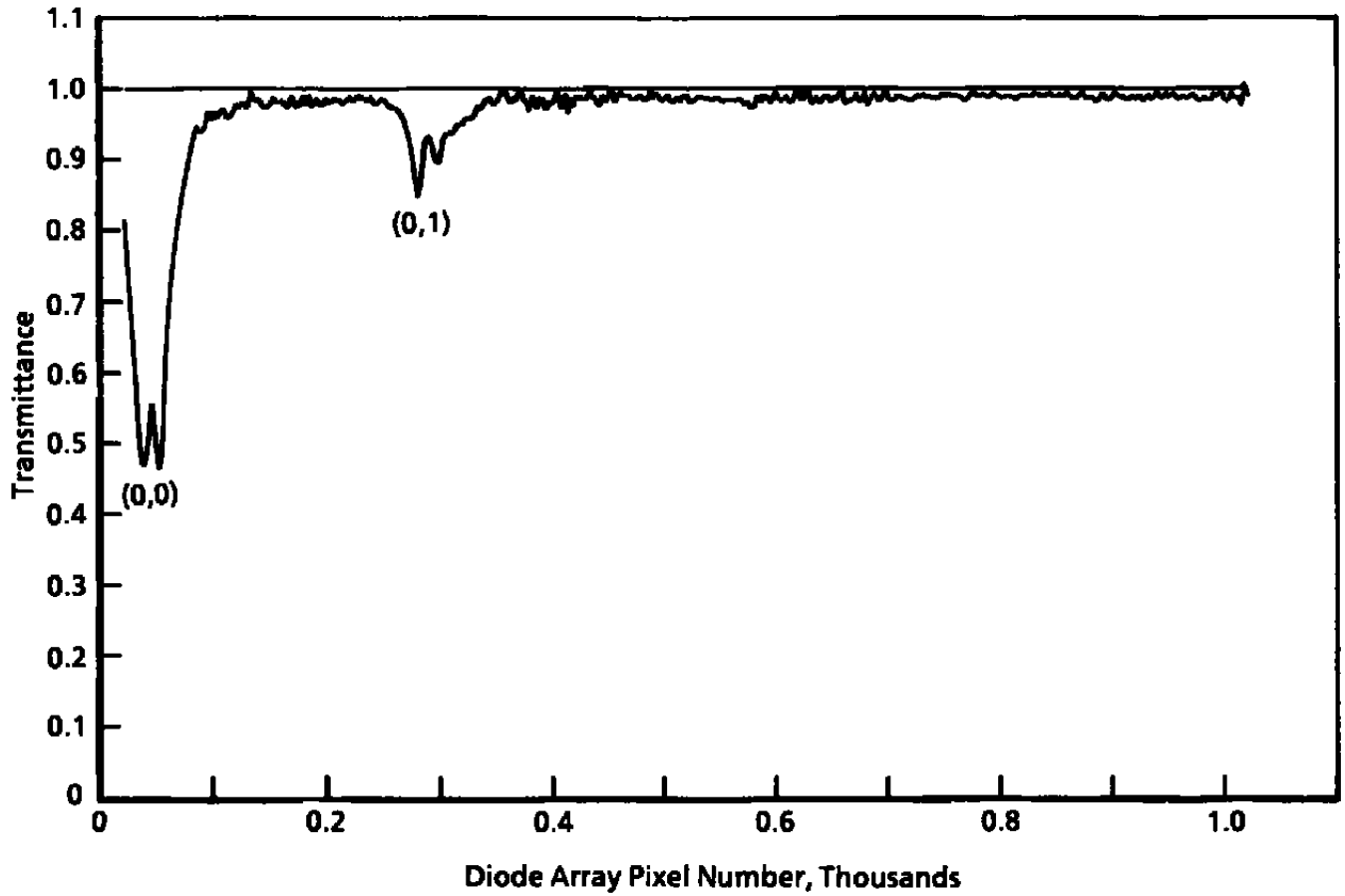

a. Spectral transmittance

Figure B-6. Spectral transmittance and a time history of the NO gamma (0,0)and (0,3) band transmittances for Test R3B2.

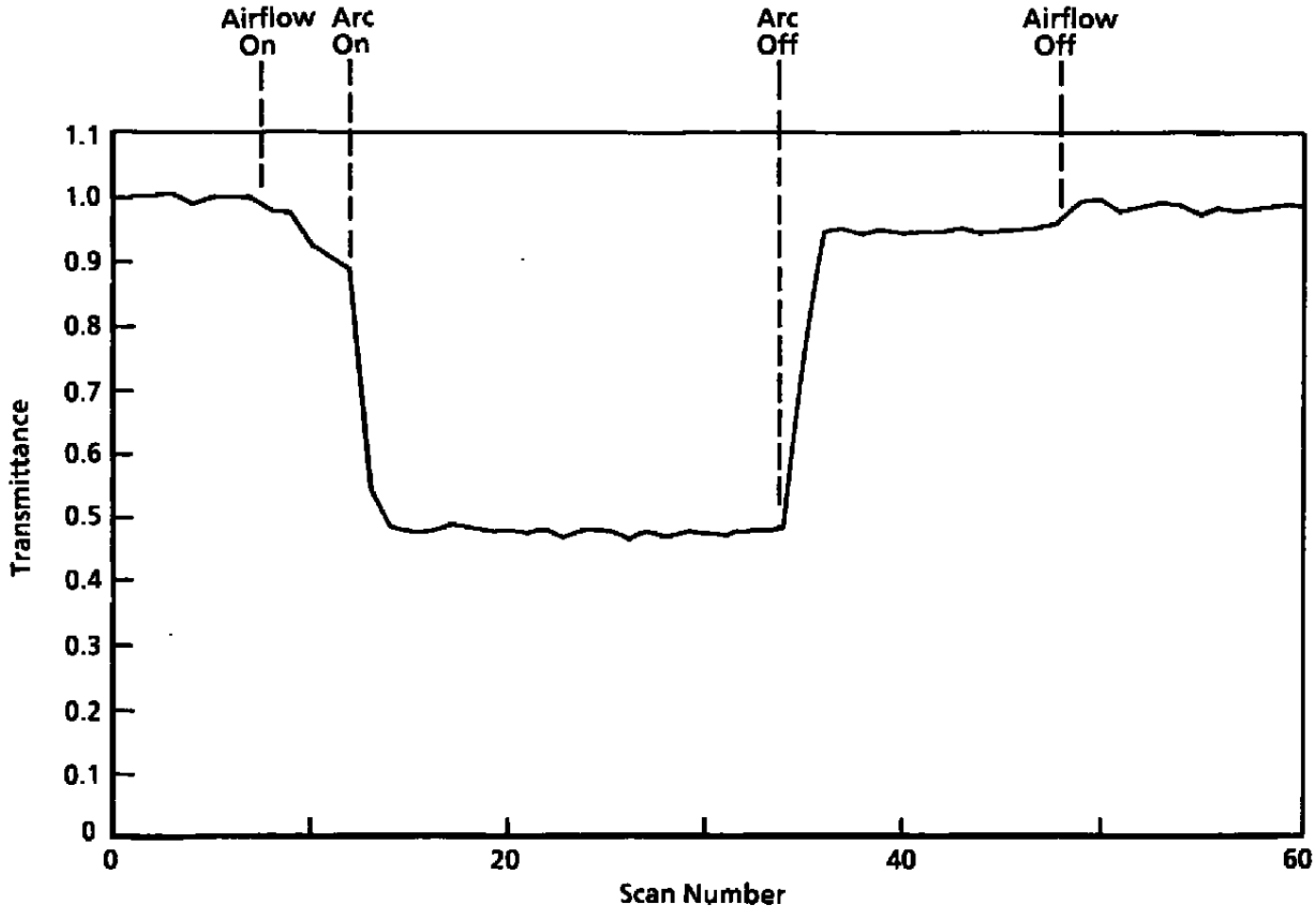

b. NO gamma (0,0) second bandhead transmittance
Figure B-6. Continued.

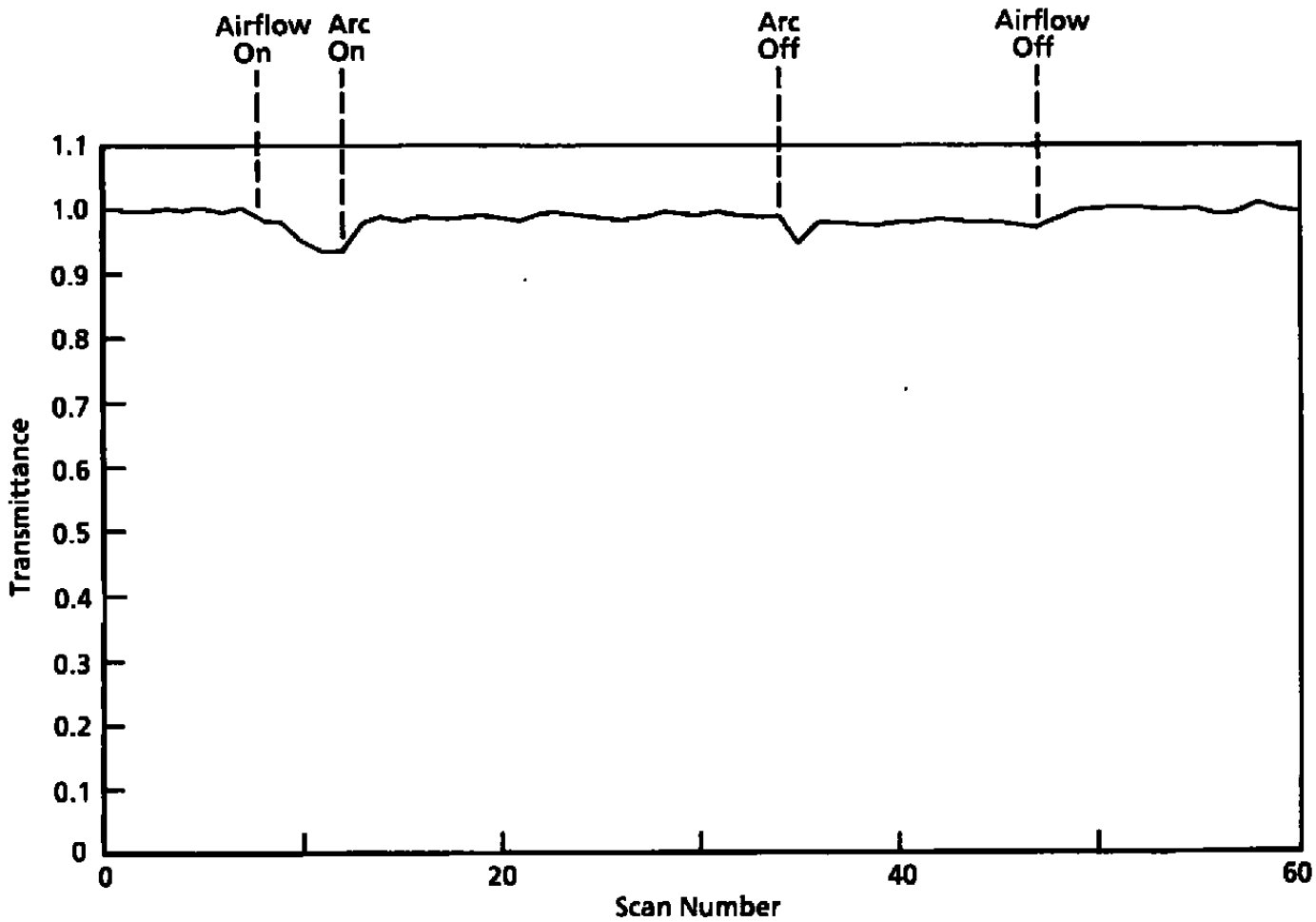

c. No gamma (0,3) second bandhead transmittance

Figure B-6. Concluded.

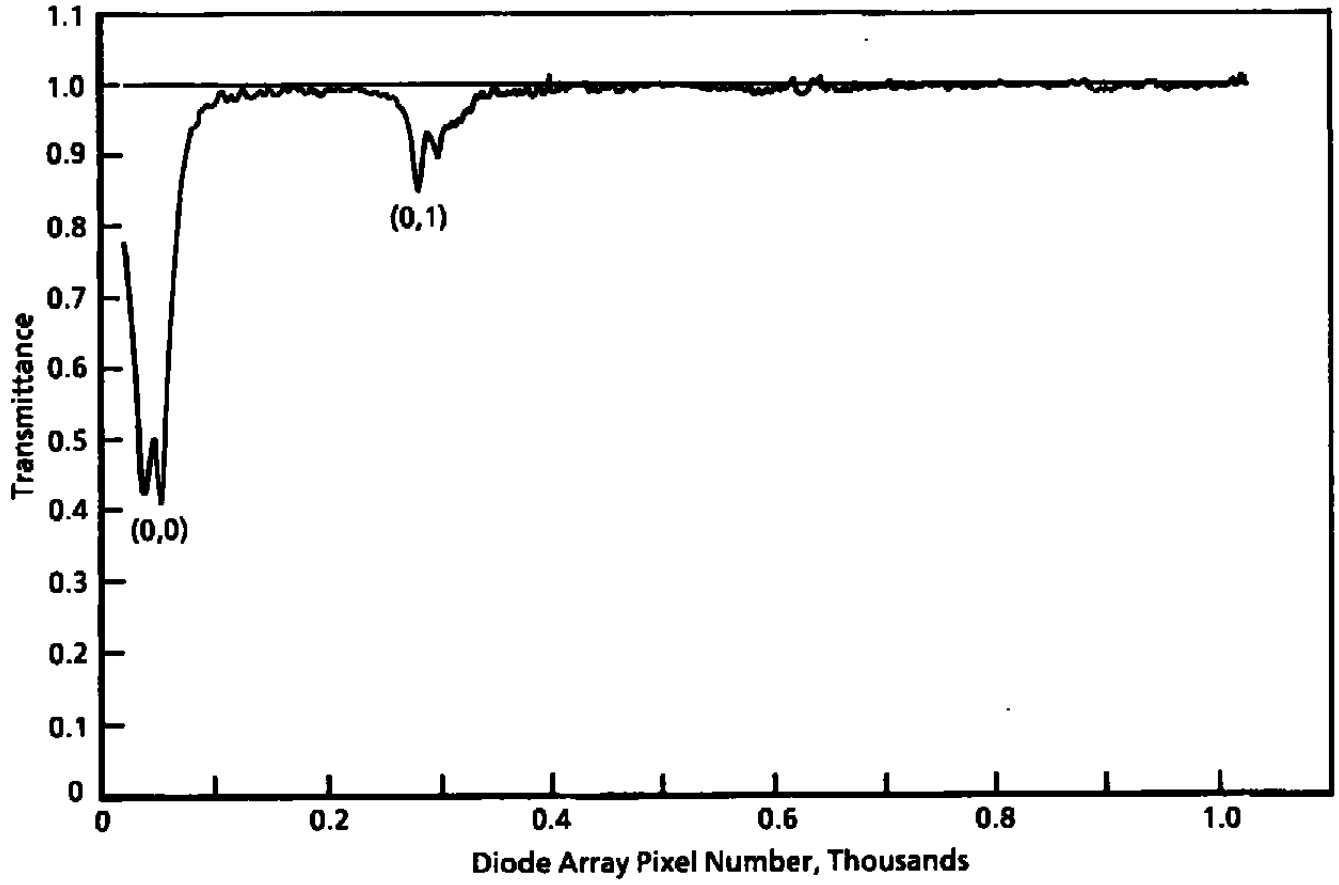

a. Spectral transmittance

Figure B-7. Spectral transmittance and a time history of the NO gamma (0,0)and (0,3) band transmittances for Test R3B3.

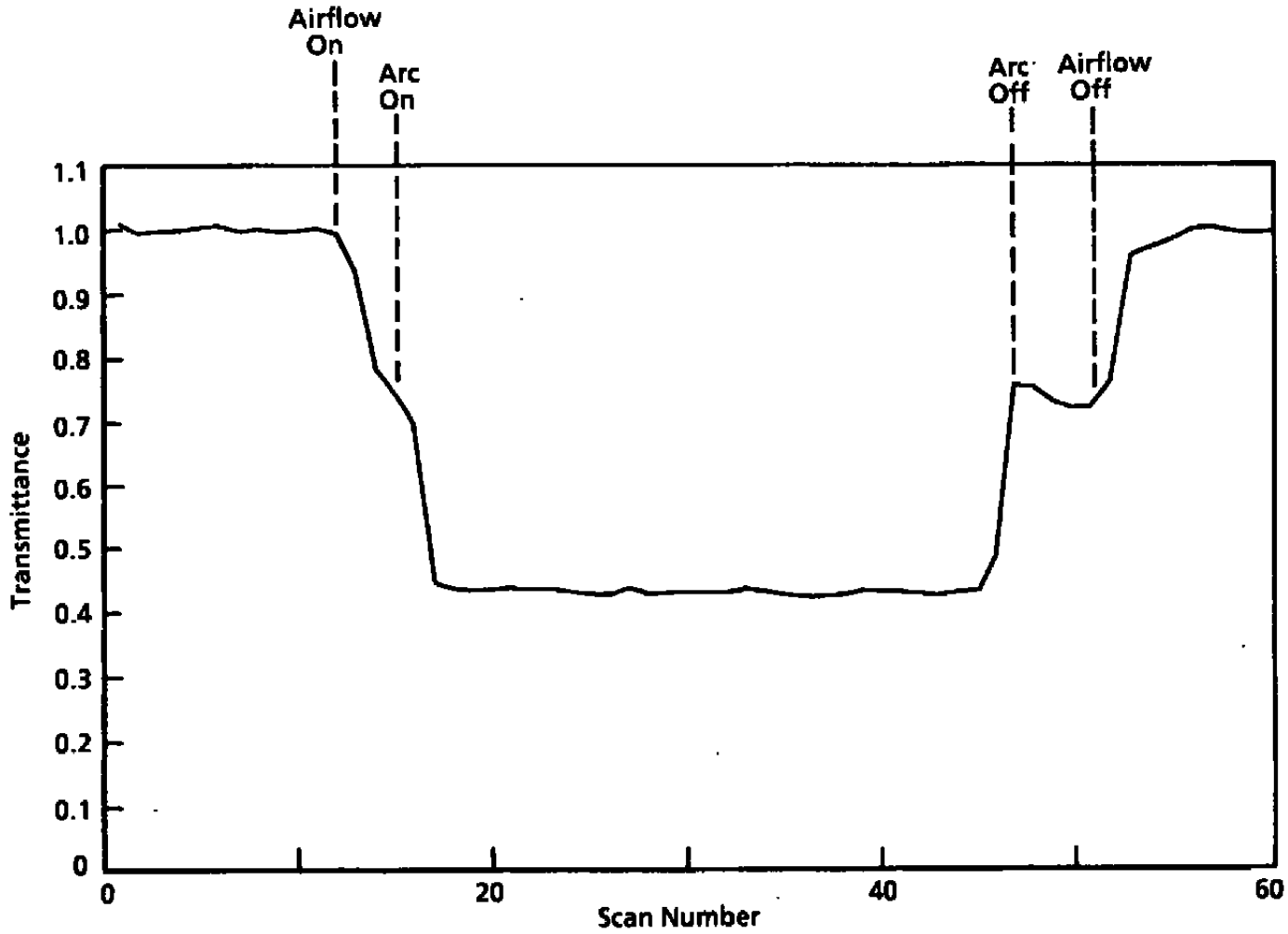

b. NO gamma (0,0) second bandhead transmittance
Figure B-7. Continued.

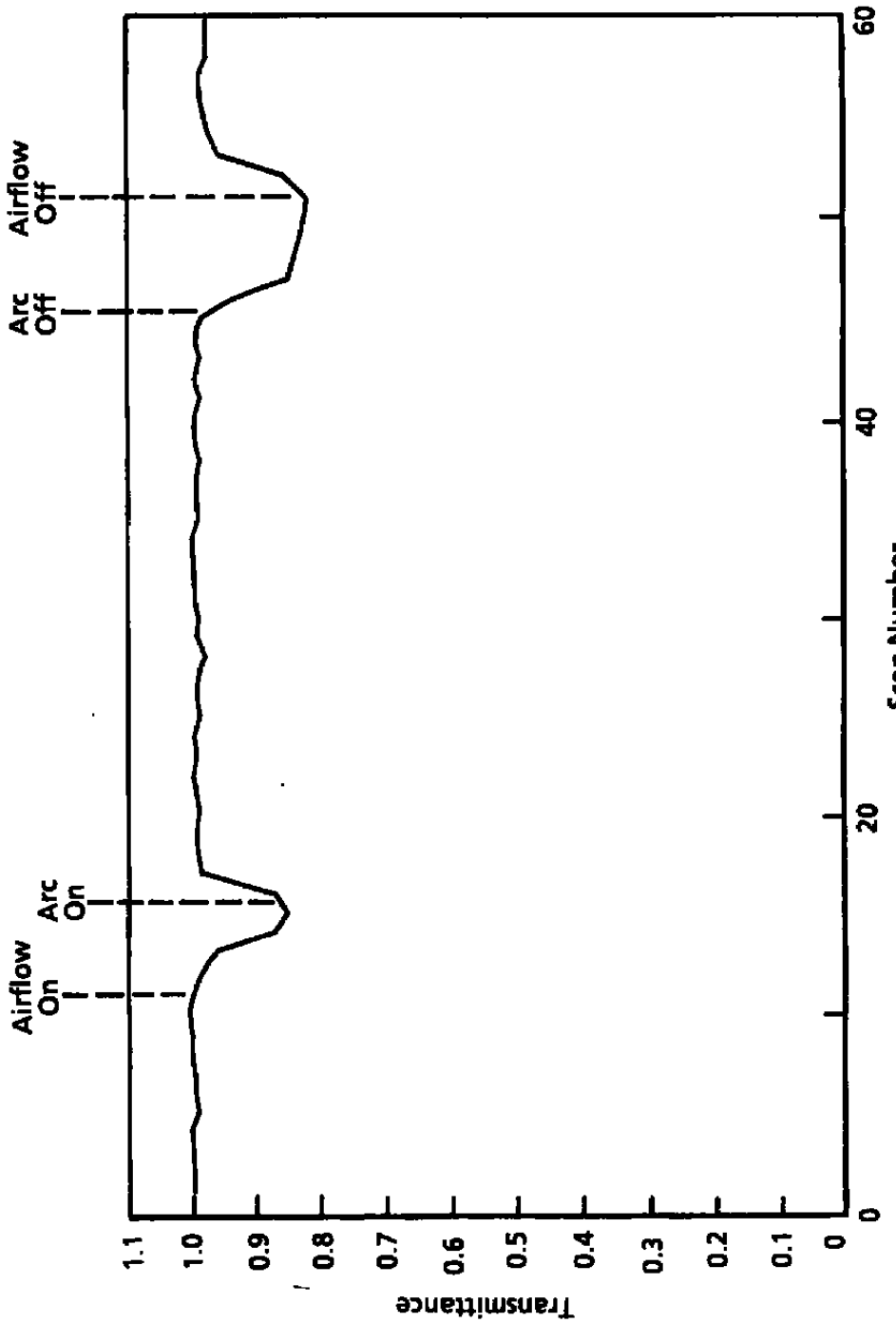

c. No gamma (0,3) second bandhead transmittance

Figure B-7. Concluded.

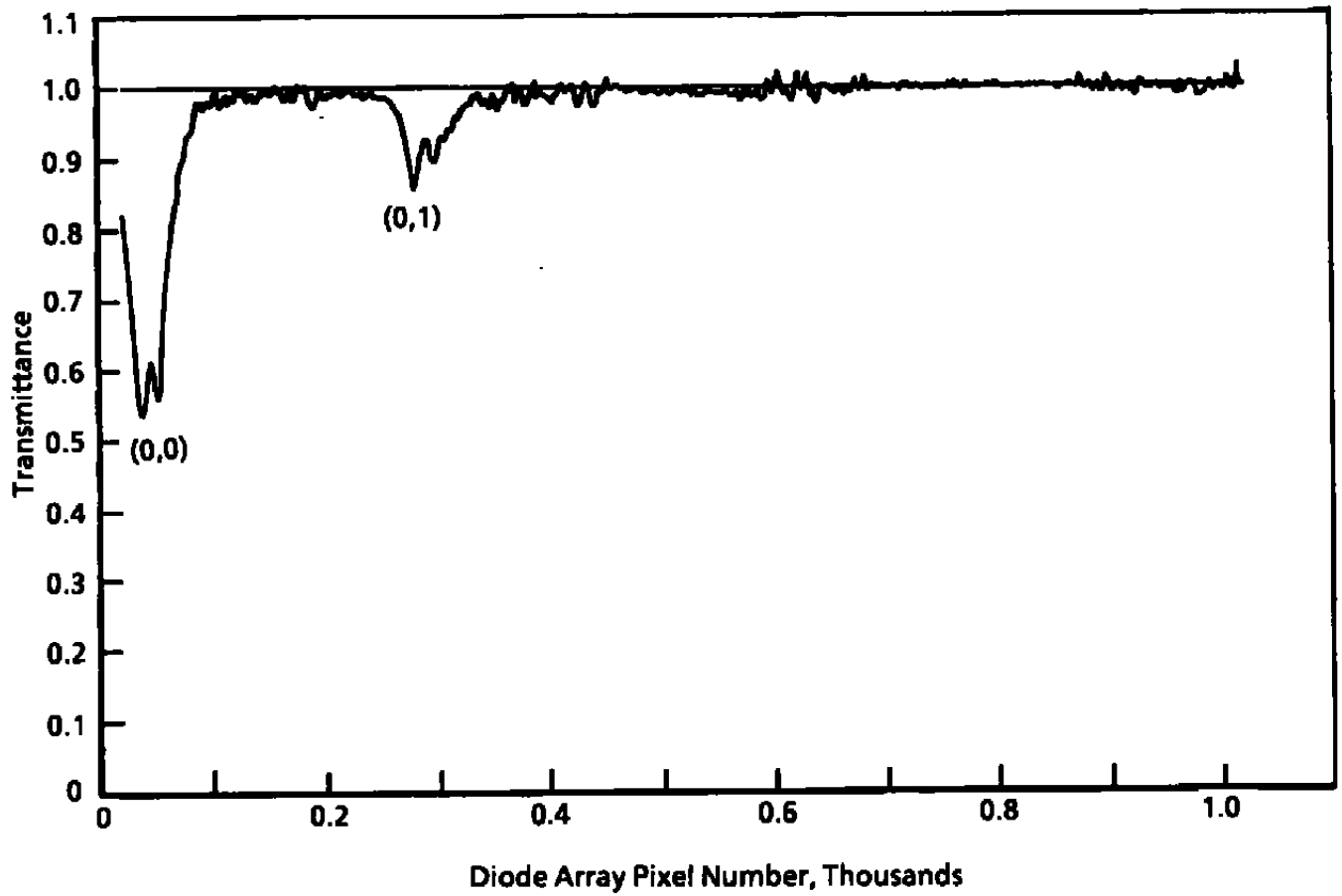

a. Spectral transmittance

Figure B-8. Spectral transmittance and a time history of the NO gamma (0,0)and (0,3) band transmittances for Test R3B4.

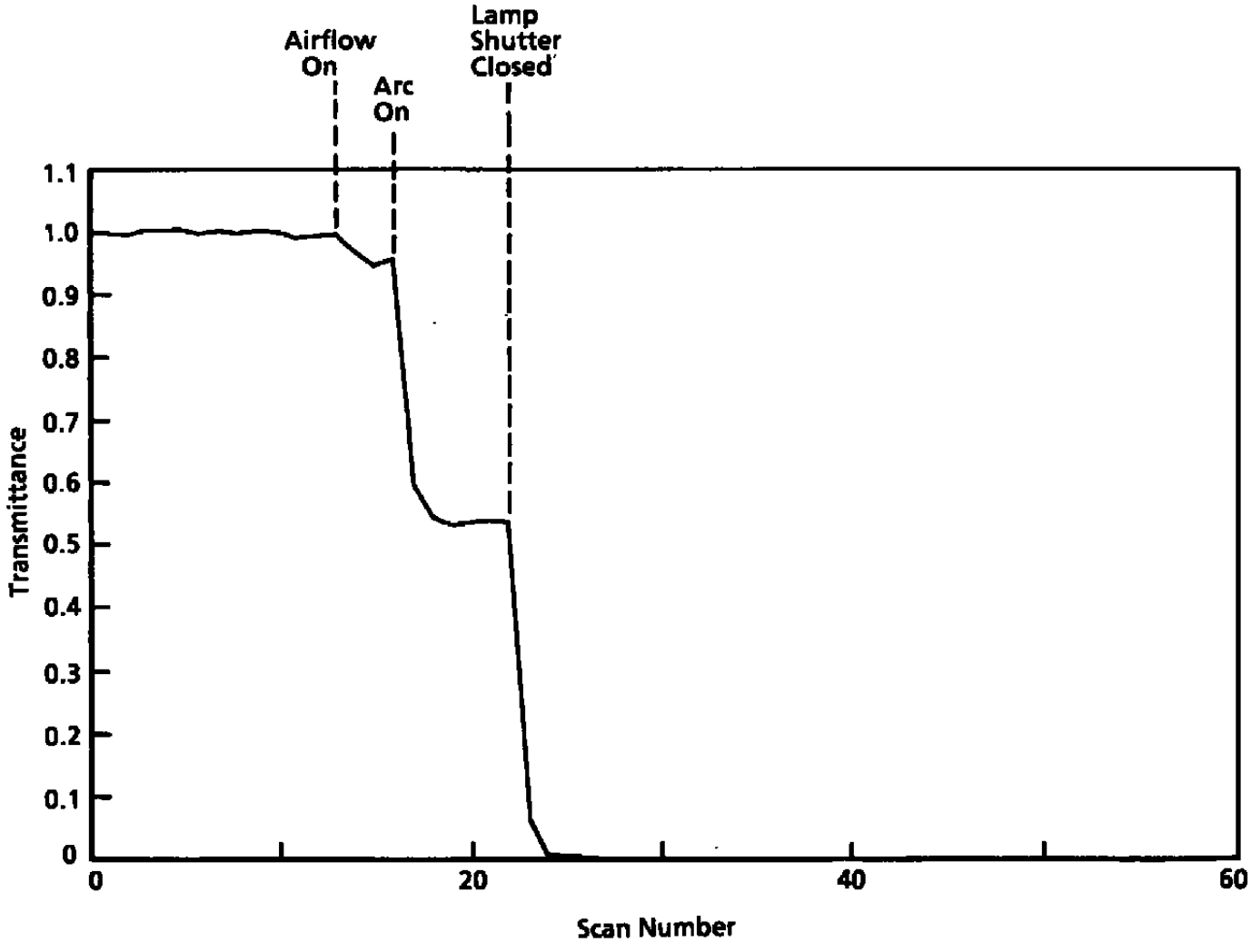

b. NO gamma (0,0) second bandhead transmittance
Figure B-8. Continued.

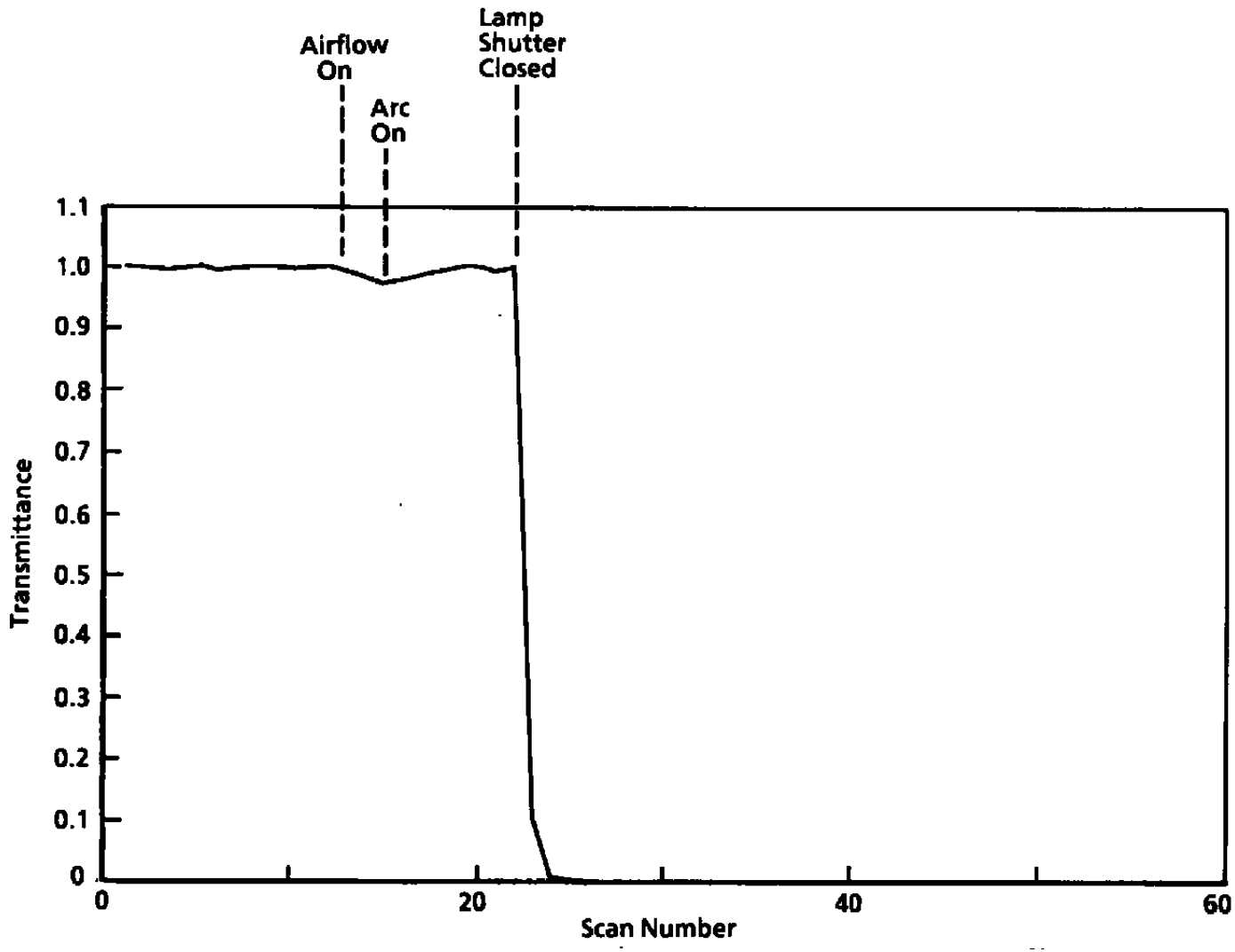

c. No gamma (0,3) second bandhead transmittance

Figure B-8. Concluded.

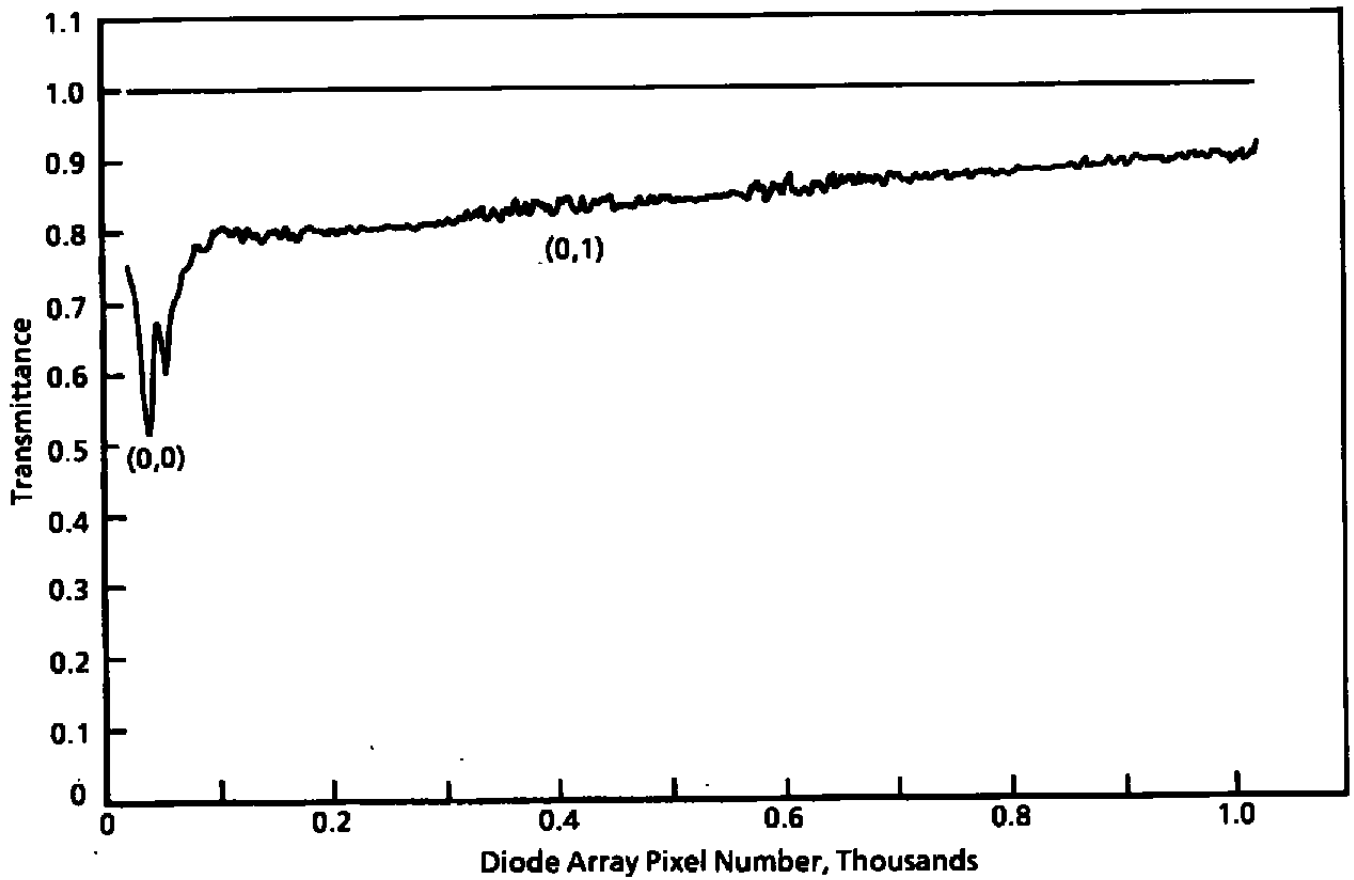

a. Spectral transmittance

Figure B-9. Spectral transmittance and a time history of the NO gamma (0,0)and (0,3) band transmittances for Test R4B1.

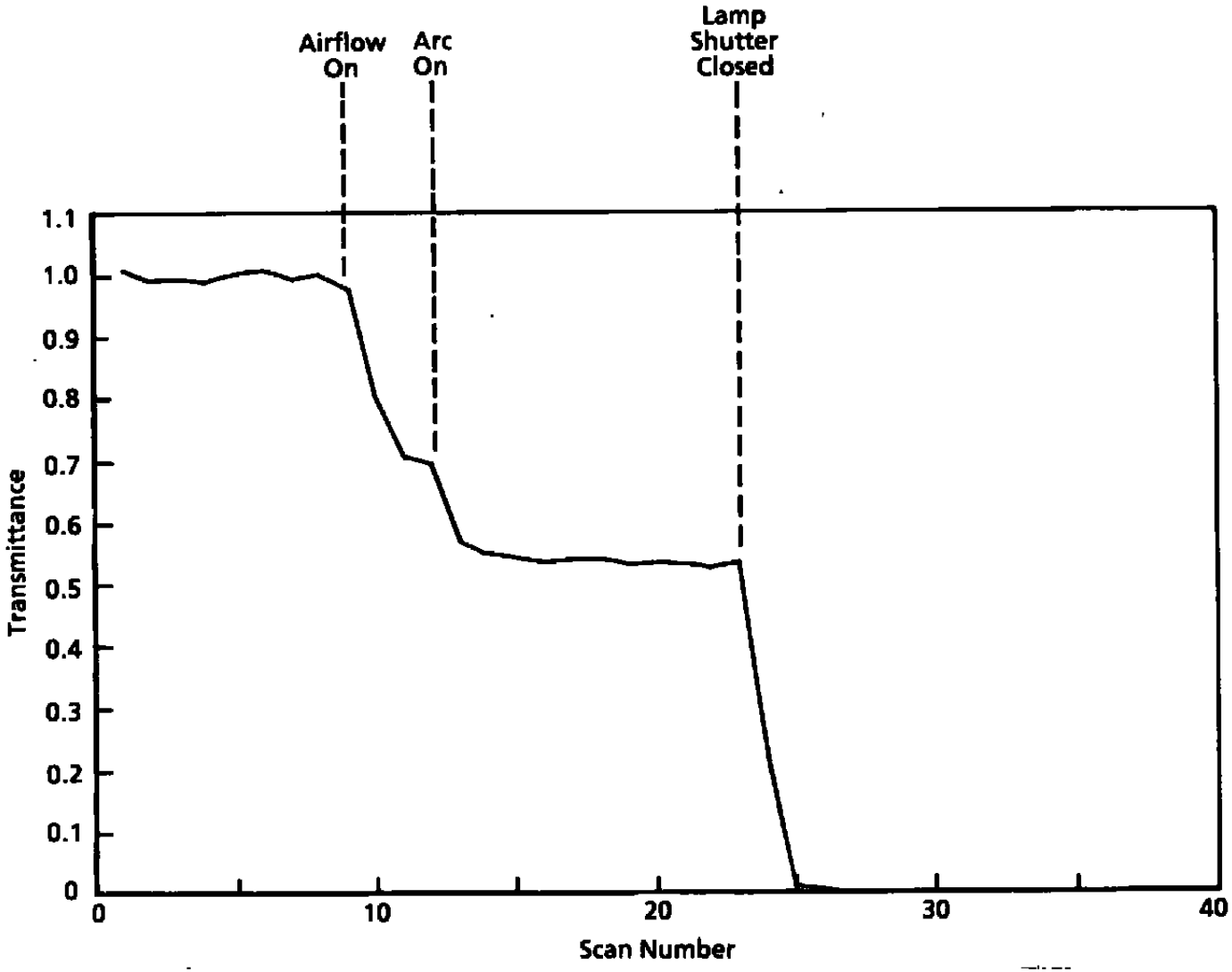

b. NO gamma (0,0) second bandhead transmittance
Figure B-9. Continued.

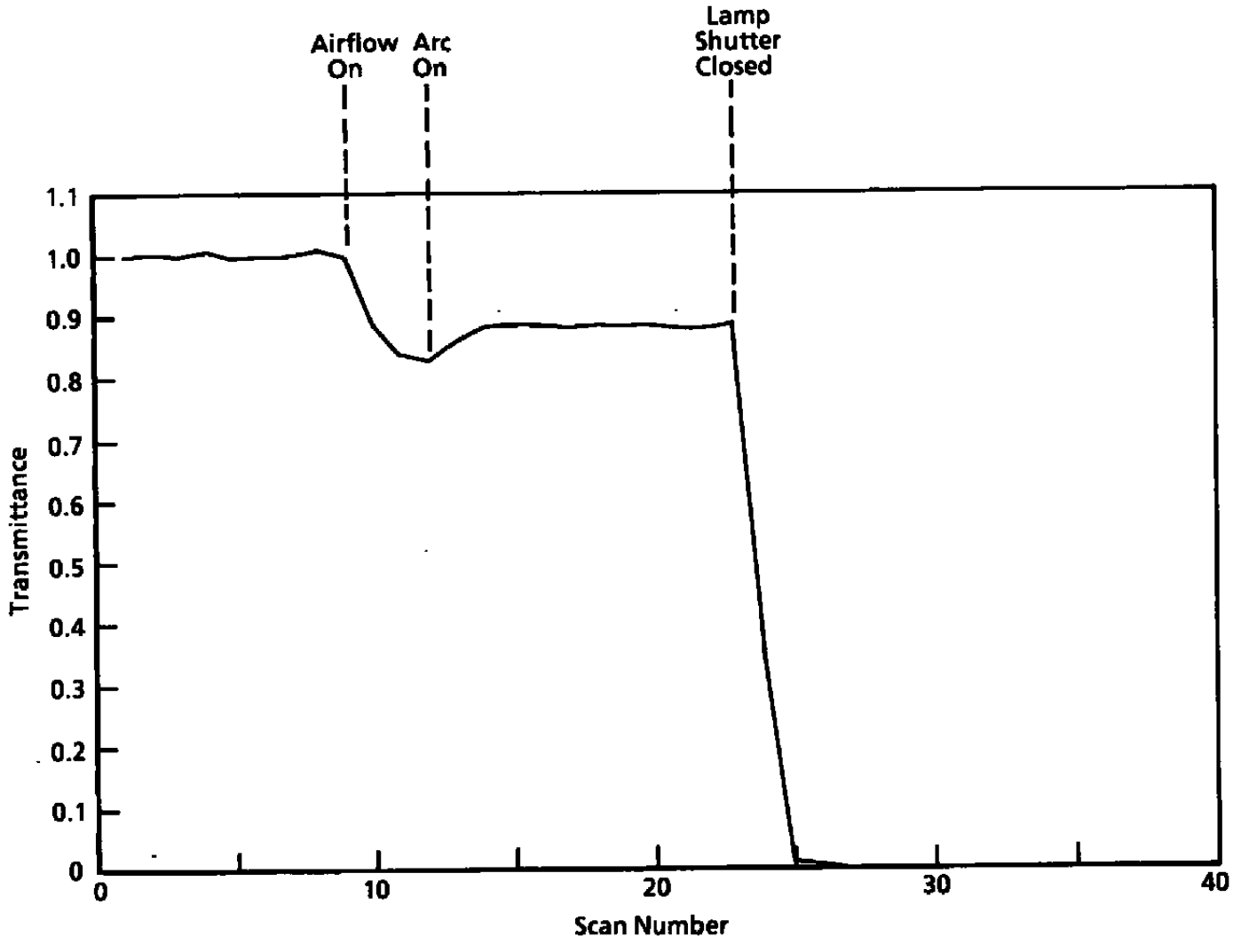

c. No gamma (0,3) second bandhead transmittance
Figure B-9. Concluded.

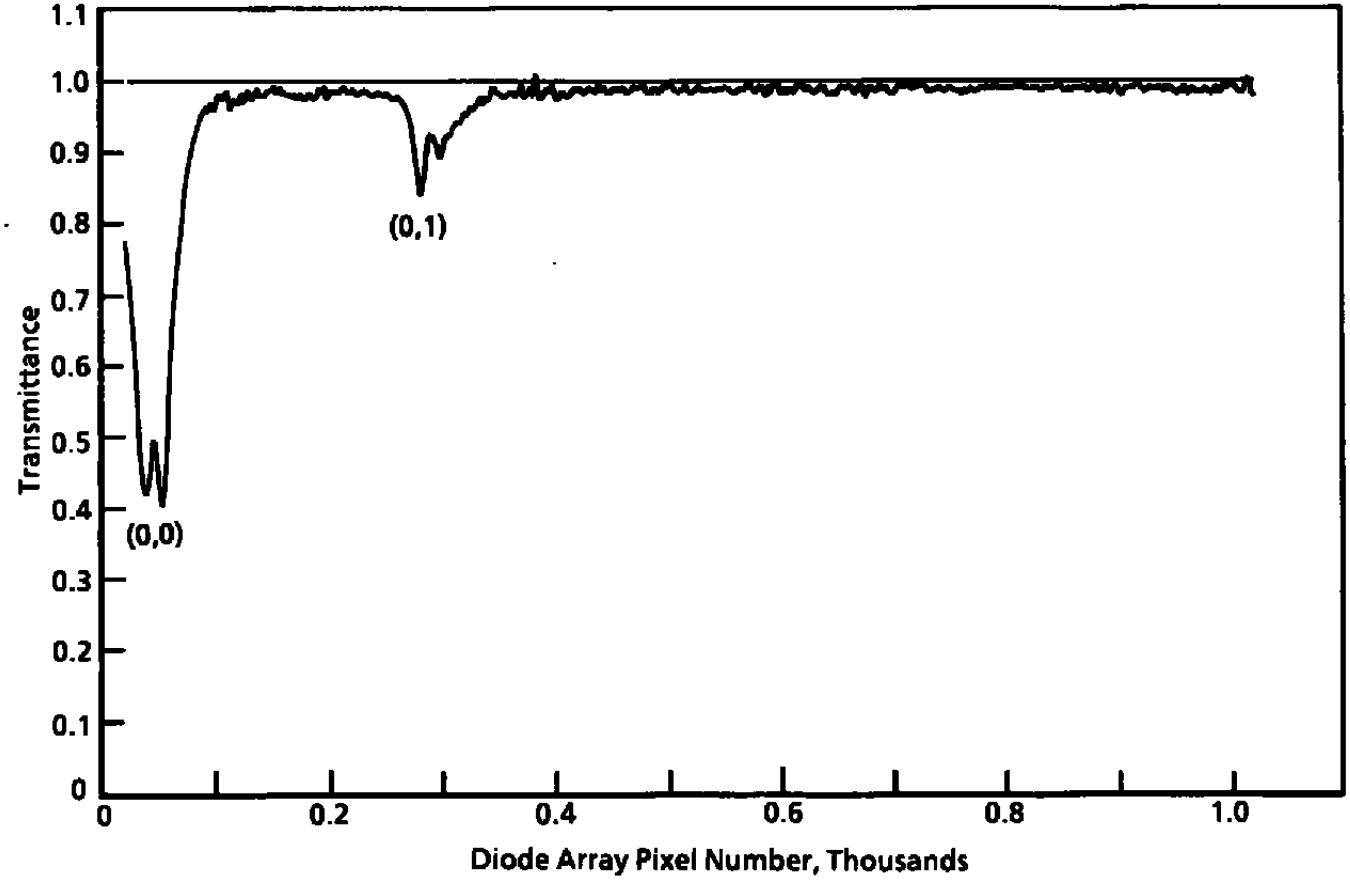

a. Spectral transmittance

Figure B-10. Spectral transmittance and a time history of the NO gamma (0,0)and (0,3) band transmittances for Test R4B2.

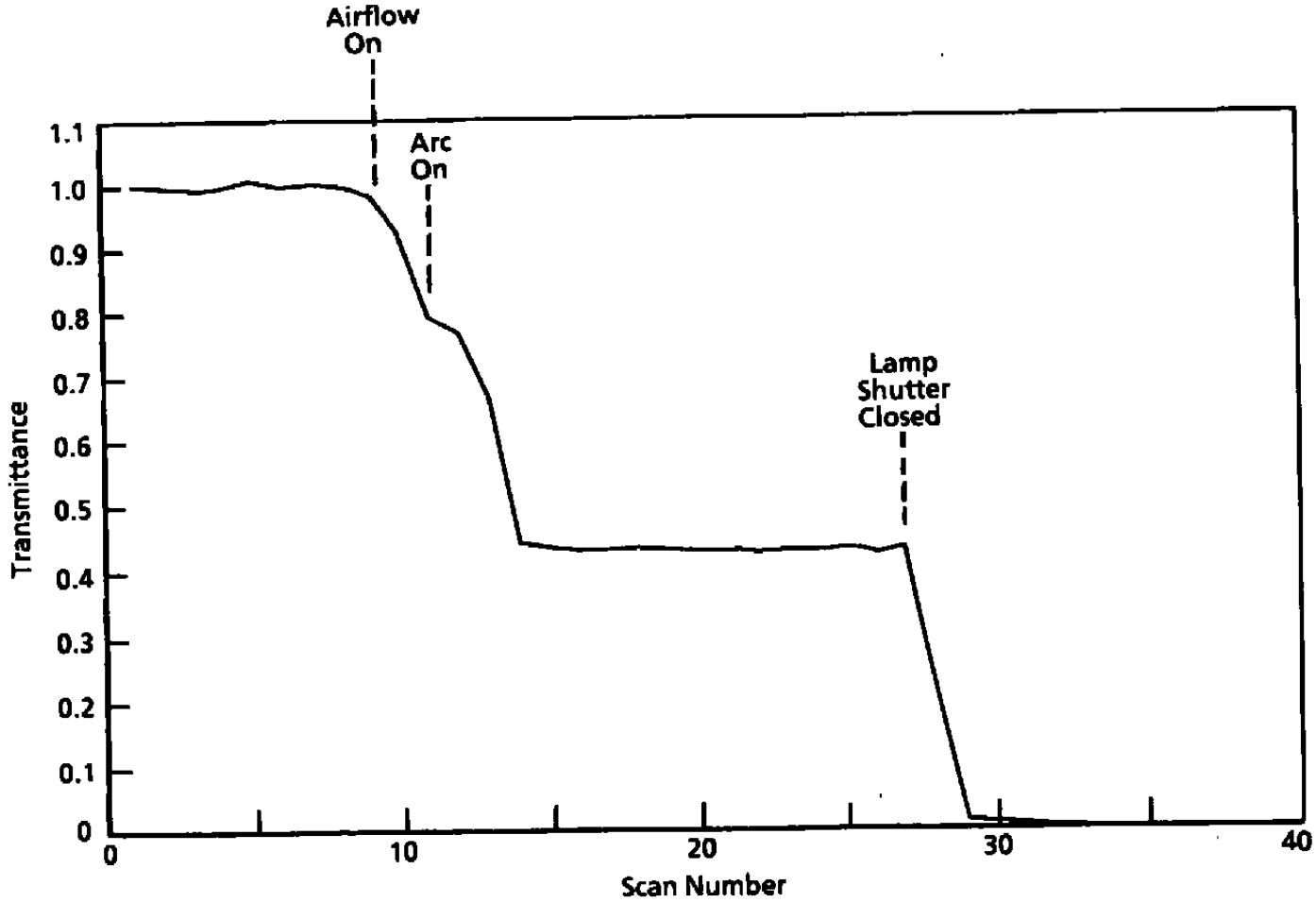

b. NO gamma (0,0) second bandhead transmittance
Figure B-10. Continued.

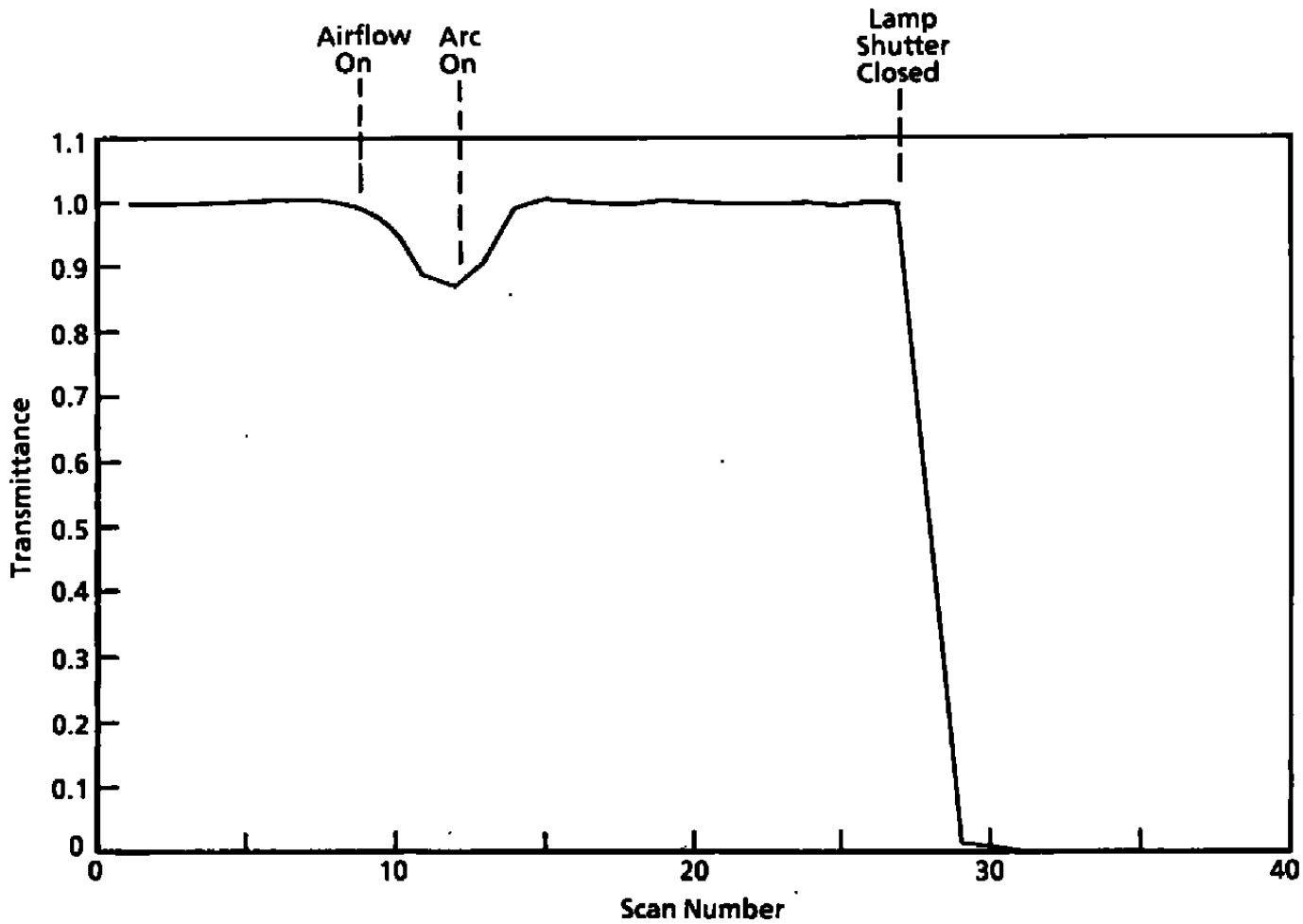

c. No gamma (0,3) second bandhead transmittance

Figure B-10. Concluded.

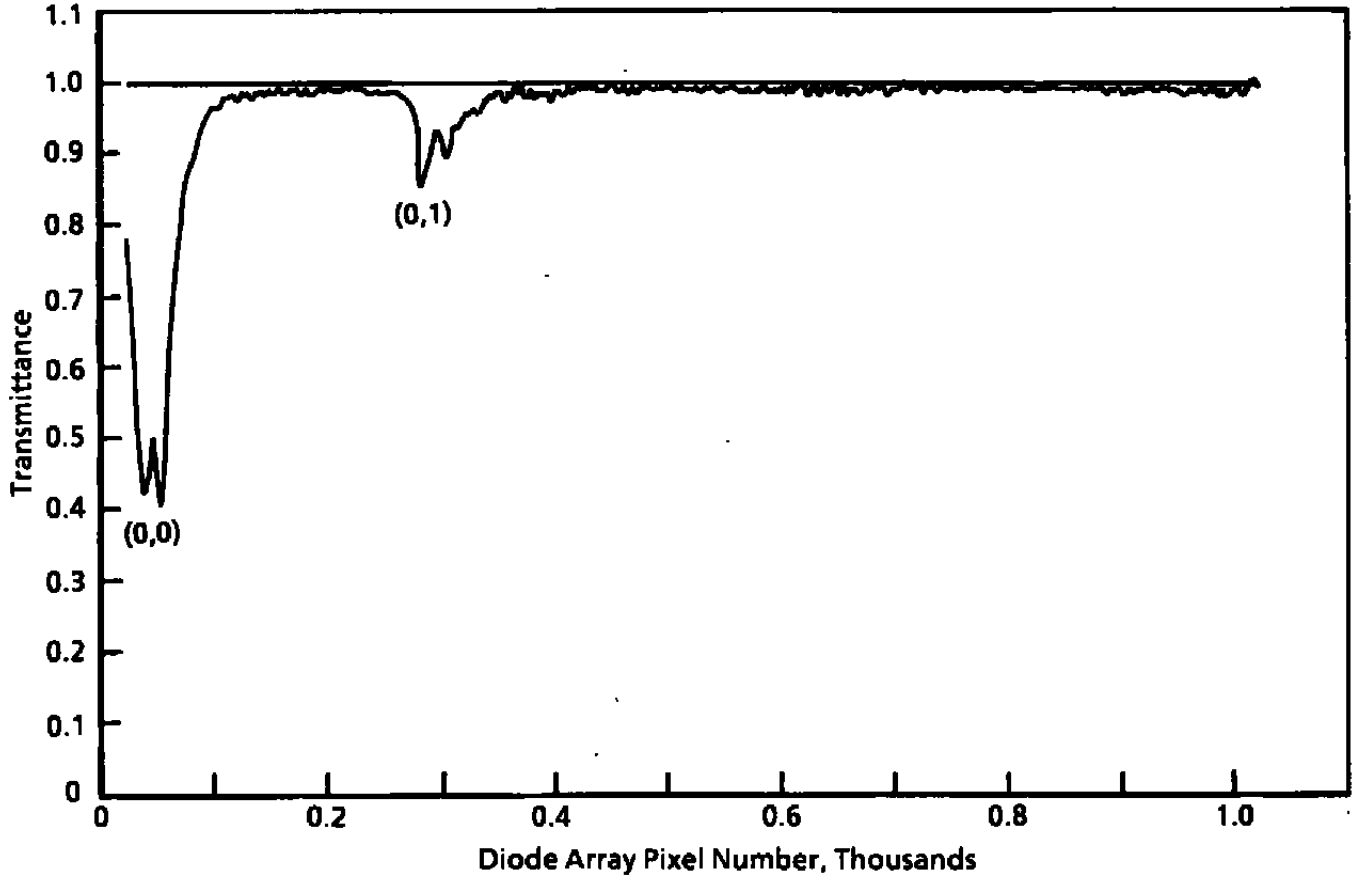

a. Spectral transmittance

Figure B-11. Spectral transmittance and a time history of the NO gamma (0,0)and (0,3) band transmittances for Test R4B3.

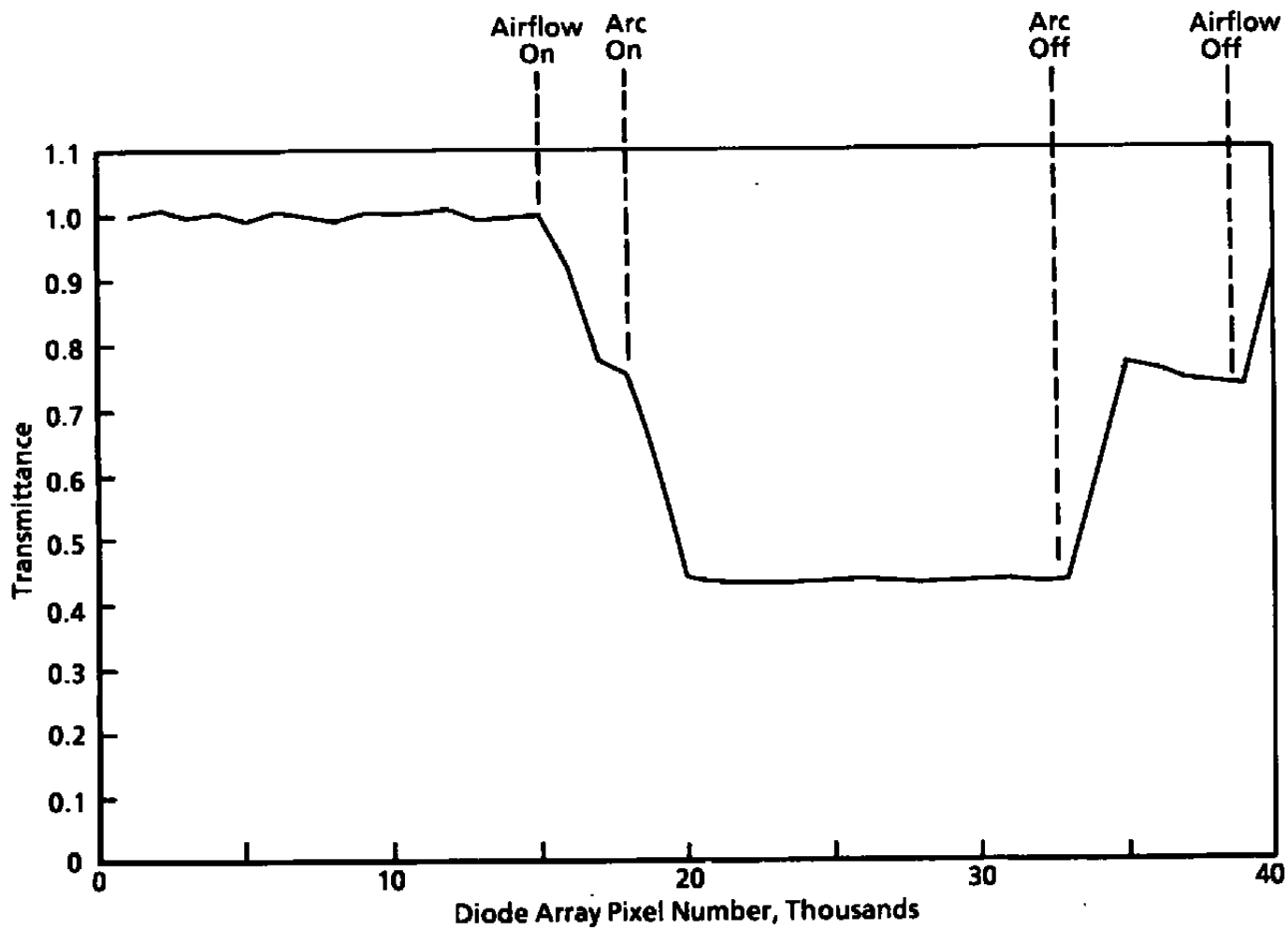

b. NO gamma (0,0) second bandhead transmittance
Figure B-11. Continued.

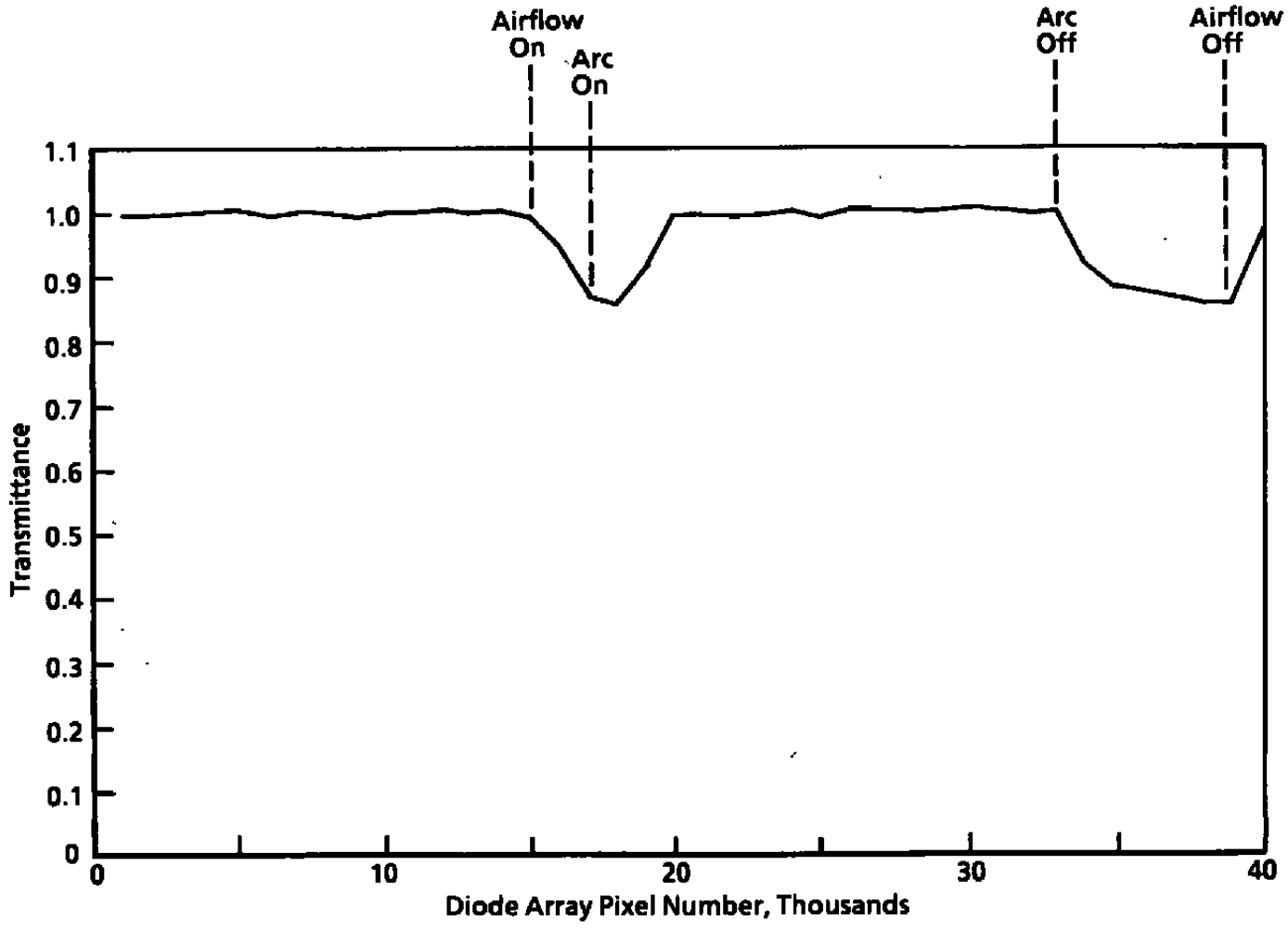

c. No gamma (0,3) second bandhead transmittance

Figure B-11. Concluded.

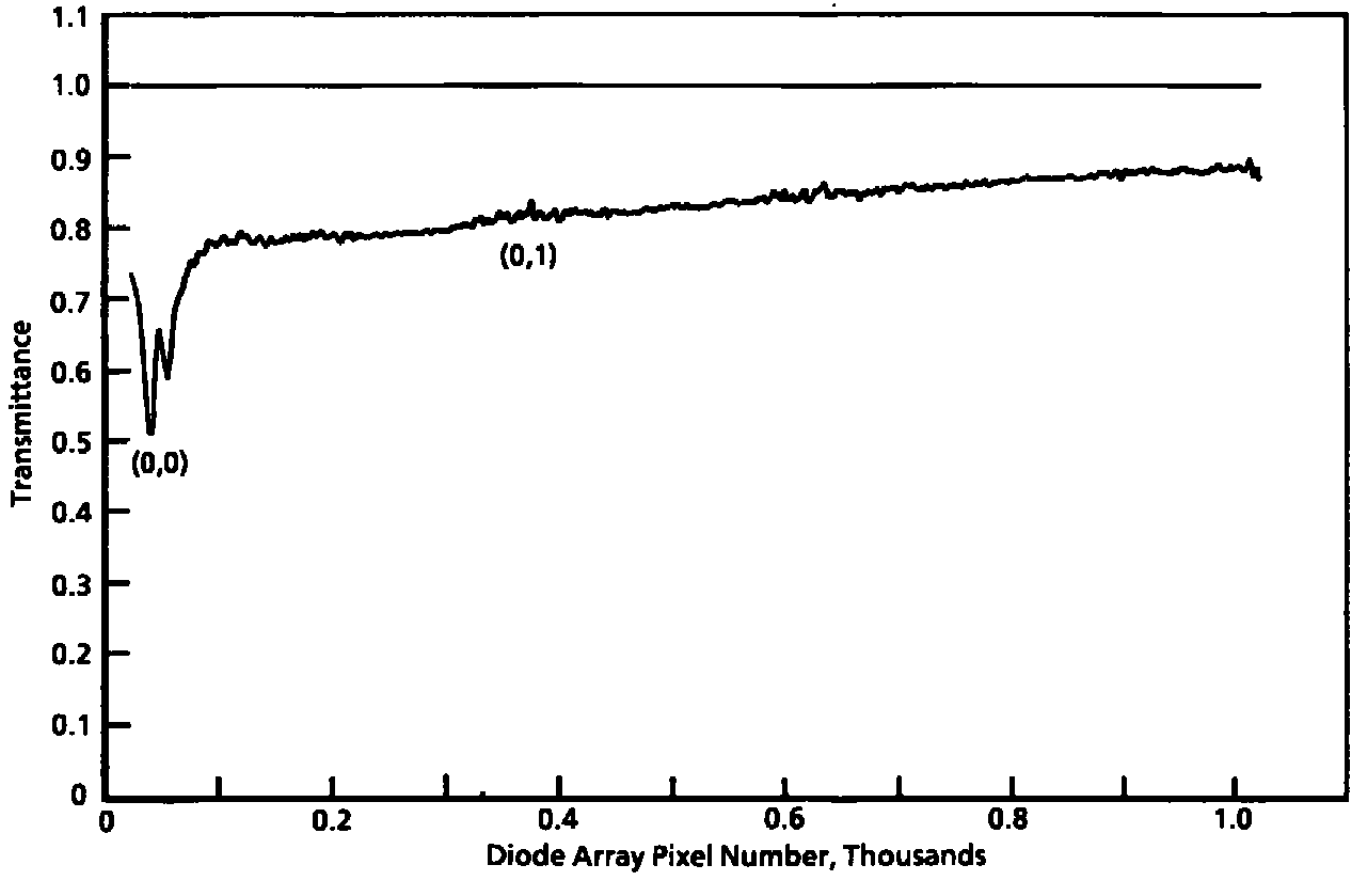

a. Spectral transmittance

Figure B-12. Spectral transmittance and a time history of the NO gamma (0,0)and (0,3) band transmittances for Test R4B4.

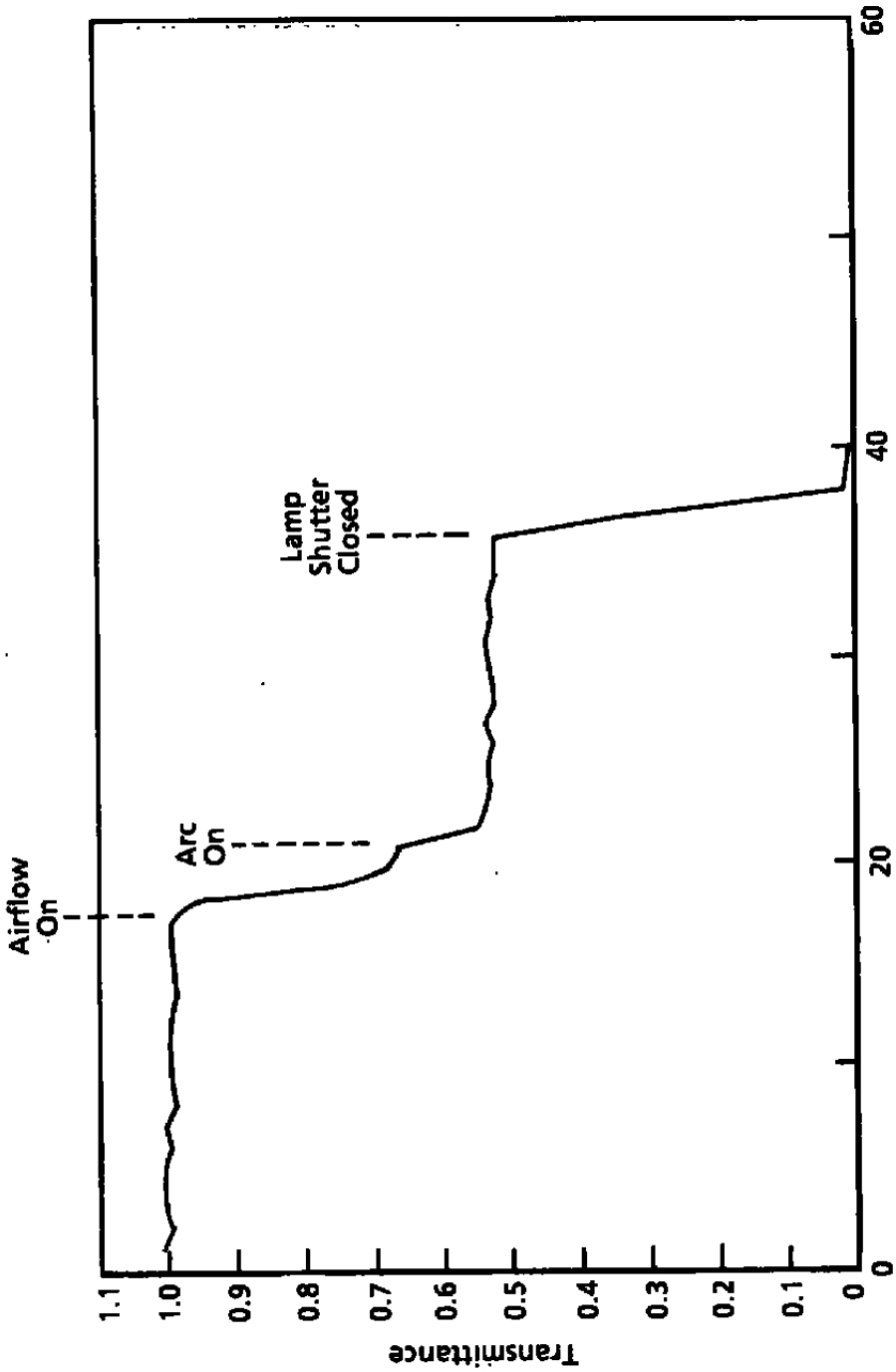

b. NO gamma (0,0) second bandhead transmittance
Figure B-12. Continued.

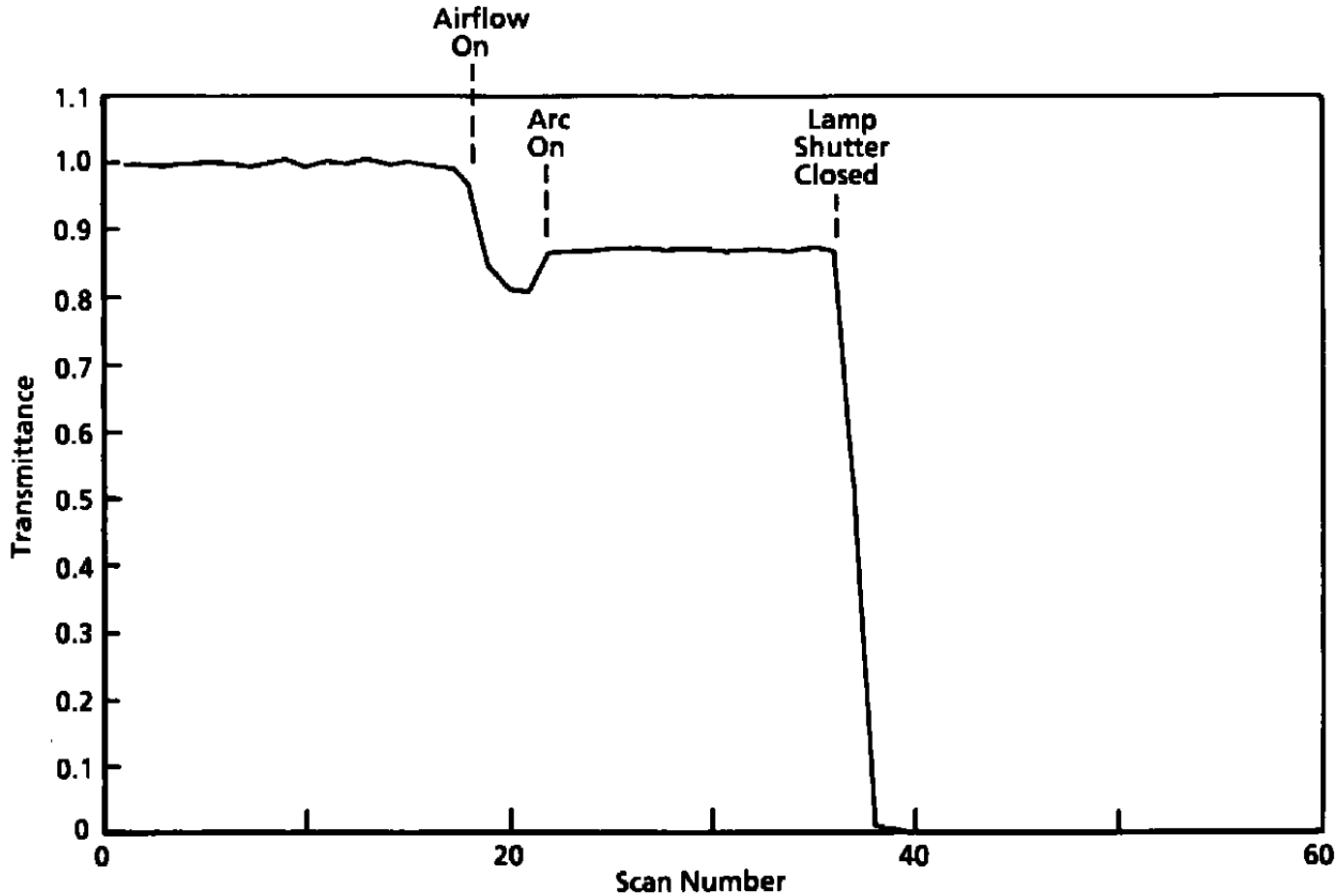

c. No gamma (0,3) second bandhead transmittance
Figure B-12. Concluded.